

MARVEL: Raster Manga Vectorization via Primitive-wise Deep Reinforcement Learning

Hao Su, Xuefeng Liu, Jianwei Niu, Jiahe Cui, Ji Wan, Xinghao Wu, Nana Wang

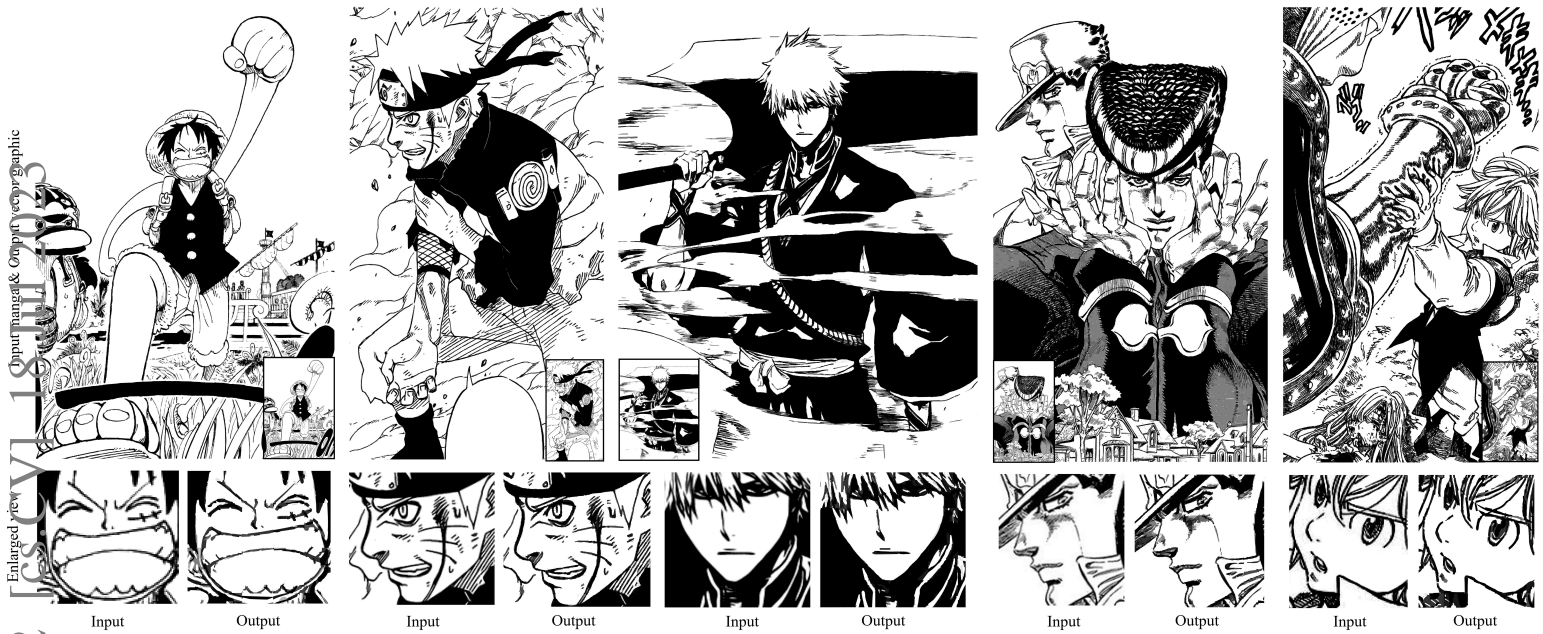


Fig. 1: Input raster mangas (black boxes) and our vectorized outputs. These vectorized mangas are displayed in PDF format that can be zoomed in freely.

Abstract—Manga is a fashionable Japanese-style comic form that is composed of black-and-white strokes and is generally displayed as raster images on digital devices. Typical mangas have simple textures, wide lines, and few color gradients, which are vectorizable natures to enjoy the merits of vector graphics, e.g., adaptive resolutions and small file sizes. In this paper, we propose MARVEL (Manga’s Raster to VECtor Learning), a primitive-wise approach for vectorizing raster mangas by Deep Reinforcement Learning (DRL). Unlike previous learning-based methods which predict vector parameters for an entire image, MARVEL introduces a new perspective that regards an entire manga as a collection of basic primitives—stroke lines, and designs a DRL model to decompose the target image into a primitive sequence for achieving accurate vectorization. To improve vectorization accuracies and decrease file sizes, we further propose a stroke accuracy reward to predict accurate stroke lines, and a pruning mechanism to avoid generating erroneous and repeated strokes. Extensive subjective and objective experiments show that our MARVEL can generate impressive results and reaches the state-of-the-art level. Our code is open-source at: <https://github.com/SwordHolderSH/Mang2Vec>.

Index Terms—Manga, Image Vectorization, Deep Reinforcement Learning.

Hao Su, Jianwei Niu, Xuefeng Liu, Jiahe Cui, Ji Wan, Xinghao Wu are with State Key Lab of VR Technology and System, School of Computer Science and Engineering, Beihang University, Beijing, 100000, China. Jianwei Niu is also with Industrial Technology Research Institute, School of Information Engineering, Zhengzhou University, Henan, 450000, China; Hangzhou Innovation Institute, Beihang University, Zhejiang, 310000, China. Corresponding author: Jianwei Niu, Email: niujianwei@buaa.edu.cn.

I. INTRODUCTION

MANGA is a fashionable Japanese-style comic form that is generally displayed as raster images on digital devices. As shown in Figure 1 and 2, mangas have simple structures, wide lines, and few color gradients which are the potential vectorizable natures. The main merits of vectorizing raster manga are two-fold. First, vector graphics are resolution-independent and readily displayed on digital devices with different resolutions. Second, for showing high-resolution contents, vector formats have higher compression ratios for storage than raster images.

Image vectorization has been studied extensively in vision, graphics, and other areas. Representative studies of image vectorization are divided into two categories. The first category of studies is based on pre-designed algorithms, which analyzes pixels and fits vector paths and graphics (e.g., [1]–[11]). The other category of studies is based on deep learning (DL) (e.g., [12]–[23]), which trains neural models to map raster images to vector parameters. However, existing DL-based approaches generally vectorize an entire image in one step, and the one-step manner limits the number of processable vector parameters. Hence, as shown in Figure 3, these approaches only work well in vectorizing simple structures (e.g, fonts, icons, sketches, logos, and emojis), and cannot vectorize mangas with complex structures.

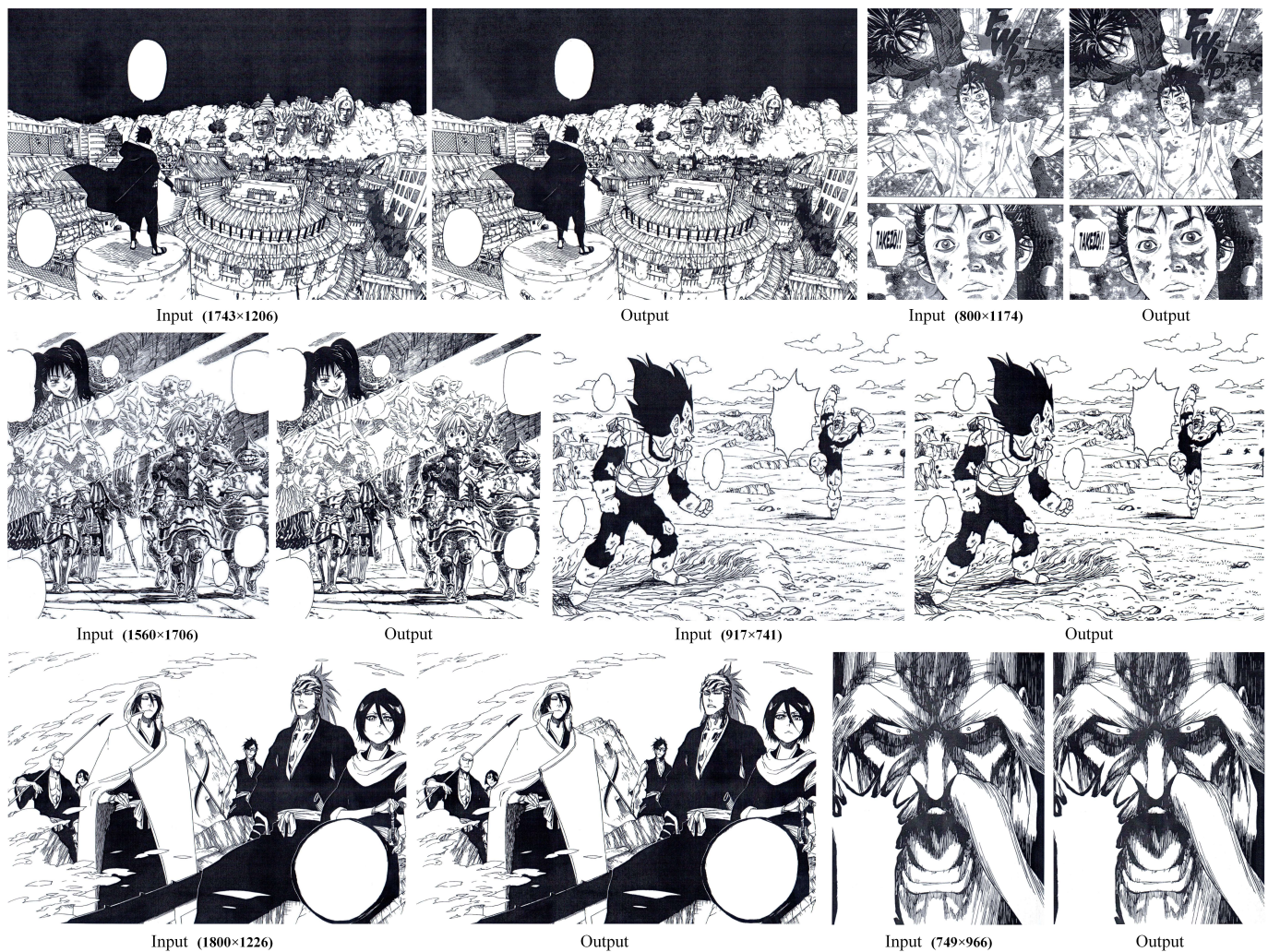


Fig. 2: Scan results of the print versions of raster inputs and our vectorized outputs¹. Our MARVEL can vectorize manga with extremely complex textures, and can effectively preserve high similarities with the raster counterparts in the print versions. The comparison in enlarged view is displayed in Figure 27, and the corresponding outputs in vector formats are shown in the supplementary material.



Fig. 3: Existing learning-based methods vectorize an entire image in a one-step manner which limits the processable vector parameters. Thus, they only have high performance in vectorizing simple textures (e.g. icons, fonts, sketches), and cannot vectorize mangas with complex structures.

To address this issue, we present *MARVEL (Manga’s Raster to Vector Learning)*, which introduces a new perspective that decomposes an entire manga into a sequence of primitives—stroke lines for achieving accurate vectorization. Employing the power of Deep Reinforcement Learning (DRL) in

stepwise processing, MARVEL can predict accurate sequential stroke lines. Since the DRL model can infinitely add stroke lines to fix inaccurate areas, MARVEL outperforms related learning-based methods for vectorizing complex structures. The merits of our approach are as follows. First, MARVEL can accurately vectorize both simple and complex textures, and can produce impressive results in (as shown in Figure 1 and 2). Second, our approach only requires supervision from readily-available raster training images without high-cost vector annotation.

In MARVEL, a DRL agent is first learned to predict the most accurate stroke line in each timestep, where the combination of all stroke lines is constrained to follow the visual content of the target manga. Then, the predicted stroke lines are converted to vector graphics by a fitting module. To improve our performance on vectorization accuracy and file size, we propose a stroke accuracy reward to optimize

¹Each sample is printed on A4 papers (210 mm×297 mm), and original resolutions of raster inputs are marked in parentheses.

stroke prediction, and a pruning mechanism to avoid producing erroneous and repeated stroke lines. Extensive subjective and objective experiments show that compared with both algorithm-based and learning-based methods, our MARVEL can produce impressive results and achieves state-of-the-art performance.

Our main contributions are summarized as follows:

- We present MARVEL, a primitive-wise method for vectorizing raster mangas by DRL. MARVEL introduces a new perspective that considers an entire manga as a sequence of primitives—stroke lines which can be decomposed from the target image to achieve accurate vectorization.
- We present a new stroke accuracy reward to improve the accuracy of predicted stroke lines, and present a pruning module to avoid erroneous strokes and reduce file sizes.
- Experiments demonstrate that our MARVEL can generate impressive results and has high performance in vectorizing numerous types of mangas with complex structures (e.g., with intensive, sparse, wide, or thin stroke lines).

II. RELATED WORK

Deep learning (DL) techniques address the single image vectorization issue utilizing the power of convolutional neural network (CNN). Below we summarize representative learning-based methods, including translative vectorization and generative vectorization.

Translative vectorization: translative methods map raster images to vector formats while preserving high visual similarities. Egiazarian et al. [12] propose a transformer-based architecture for translating technical line drawings to vector parameters. Gao et al. [14] produce parametric curves utilizing the extracted image features and a designed hierarchical recurrent network. Guo et al. [24] divide the input image into key curves by a trained CNN, and then reconstruct the topology at junctions by predicting the line connectivity. For vectorizing floorplans, Liu et al. [16] first train a CNN to convert an image to junctions, and then address an integer program that obtains the vectorized floorplans as a set of architectural primitives. For line-art images, Mo et al. [25] propose a framework of recurrent neural network that can produce vectorized line drawings. Reddy et al. [13] propose Im2Vec, a method based on variational autoencoder to predict vectorization parameters of input images, and the network can be trained without vector supervision. Moreover, there is a special method LIVE [26] that is not a typical learning-based method, which fits vector curves iteratively using a neural optimizer without training any model. LIVE requires hundreds of iterations to fit each vector curve and spends more time than vectorization methods using a trained model.

Generative vectorization: the goal of generative models is to predict vector parameters by some heuristic inputs (e.g., sketches, texts, numbers, conditional parameters), where no accurate similarities are required between inputs and outputs. SketchRNN [27] encodes the input sketches to pen positions and states, and a recurrent neural network is trained to predict

a new sketch. Similar to SketchRNN, Sketchformer [28] adopts a framework to encode vector form sketches using the transformer. SVG-VAE [29] fixes the weights of pre-trained variational auto encoder weights and trains a decoder to predict vector parameters from the latent variable. DeepSVG [30] shows that the hierarchical networks are useful to reconstruct diverse vector graphics, and do well in interpolation and generation tasks. For font glyphs vectorization, methods [31], [32] can produce results from partial observations in a low-resolution raster domain. Li et al. [33] present a differentiable rasterizer to edit and produce vector parameters by raster-based target functions and machine learning.

Existing learning-based methods focus specifically on vectorizing simple contents (e.g., fonts, numbers, sketches, line-drawings), since their neural models vectorize an entire image in a one-step manner which limits the number of processable vector parameters. Unlike these methods, our MARVEL considers a complex image as a combination of vector primitives—stroke lines, and produces accurate primitives using the DRL’s merit, i.e., predicting vector parameters in a stepwise manner.

There are also some studies that involve the simplification or beautification [34]–[43] of line-art (e.g., manga, sketch), which is a crucial step for migrating raster images to the vector domain. Amit Shesh and Baoquan Chen [44] propose an approach for simplifying 2D/3D line drawings by creating and managing a time-coherent hierarchy. Smart Scribbles [45] introduce a scribble-based interface for user-guided segmentation of sketchy drawings. Liu et al. [41] propose a novel approach to simplify sketch drawings, which makes the first attempt in incorporating the law of closure into the semantic analysis of the sketches. For simplifying manga drawing, Li et al. [34] propose a tailored deep network framework for extracting structural lines from mangas with arbitrary screen patterns.

III. METHOD

A. Overview

Given a raster manga M , our MARVEL is modeled as a function Ψ to generate a vector graphic $\mathcal{V} = \Psi(M)$, and \mathcal{V} is similar to M visually. As shown in Figure 4, MARVEL Ψ is composed of two phases, the learning phase Ψ_l (Figure 4 left) and the vectorization phase Ψ_v (Figure 4 right). Ψ_l is designed to learn a DRL model for decomposing M to a sequence of stroke lines. Specifically, following the visual content of M , a DRL agent is trained to predict an action sequence $\mathcal{A} = \Psi_l(M) = \{a_0, a_1, \dots, a_t\}$, and \mathcal{A} can be rendered to a sequence of stroke lines $\mathcal{L} = \{l_0, l_1, \dots, l_t\}$ by a drawing model \mathcal{D} , $l_t = \mathcal{D}(a_t)$. Meanwhile, the combination of strokes in \mathcal{L} are constrained to compose M visually. Ψ_v is designed to translate \mathcal{A} to the vector form \mathcal{V} . That is, leveraging the well-trained DRL agent, we predict the action sequence \mathcal{A} , and then fit \mathcal{A} to vector graphic \mathcal{V} by a fitting module.

We will detail Ψ_l and Ψ_v in Section III-B and Section III-C respectively. Table I summarizes the key notations used throughout the paper.

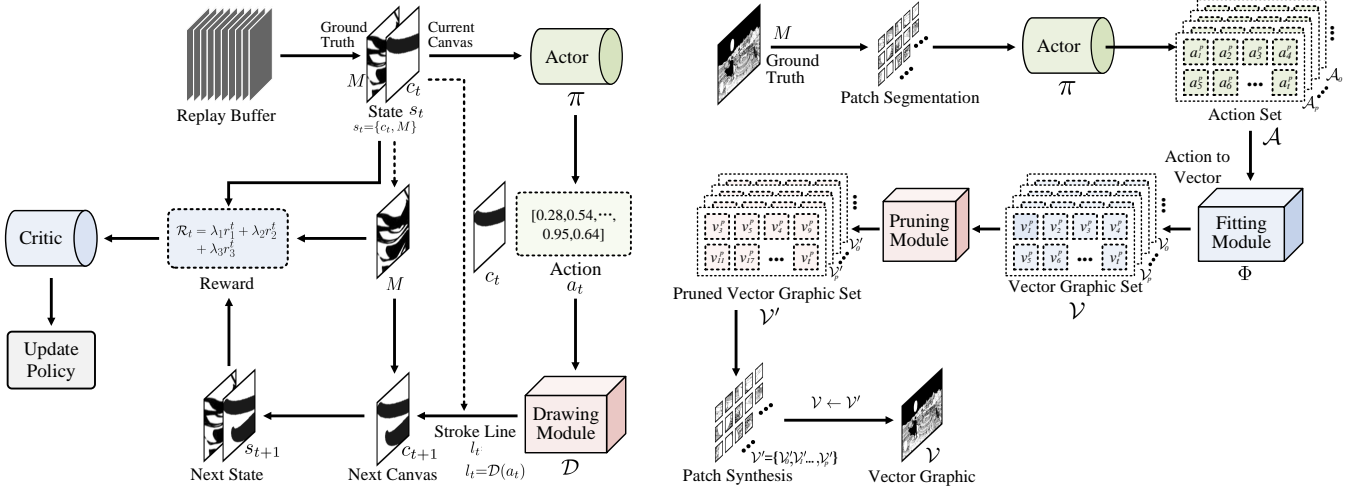


Fig. 4: System Pipeline. Given a raster manga M , our method maps M to a vector graphic \mathcal{V} with high visual similarity. **Left:** the learning phase Ψ_l aims to learn a DRL model to predict an action sequence $\mathcal{A} = \Psi_l(M)$, and \mathcal{A} can be rendered to a stroke line sequence \mathcal{L} which is encouraged to compose M visually. **Right:** the vectorization phase Ψ_v aims to translate action sequence \mathcal{A} to vector format \mathcal{V} .

TABLE I: Summary of Notations

Name	Description
M	The input raster manga (ground truth).
\mathcal{V}	The output vector graphic by vectorizing M , consisting of a sequence of vectorized strokes, $\mathcal{V} = \{v_0, v_1, \dots, v_t\}$.
\mathcal{A}	The sequence of actions, $\mathcal{A} = \{a_0, a_1, \dots, a_t\}$.
\mathcal{L}	The sequence of stroke lines, $\mathcal{L} = \{l_0, l_1, \dots, l_t\}$.
\mathcal{D}	The drawn module used to render a_t to l_t , $l_t = \mathcal{D}(a_t)$.
a_t	The t -th action predicted by agent π .
l_t	The t -th stroke line translated by a_t .
v_t	The t -th vectorized stroke line corresponding to l_t .
c_t	The t -th canvas produce by rendering stroke lines, $c_{t+1} = c_t + l_t$. The initial canvas c_0 is blank.
s_t	The t -th state that contains c_t and M , $s_t = (c_t, M)$.
p	The number of patches.
k	The maximum number of stroke lines, i.e., the maximum timestep of the DRL model.

B. Learning Phase

The goal of Ψ_l is to train a DRL agent π to predict an optimal action sequence $\mathcal{A} = \{a_0, a_1, \dots, a_t\}$. In each timestep t , an action $a_t = \pi(s_t)$ is predicted by the observed current state s_t , and a_t can be rendered to a stroke line $l_t = \mathcal{D}(a_t)$ by the drawing module \mathcal{D} . All stroke lines are rendered on a blank canvas sequentially, and the rendered canvas is constrained to be similar to M .

To improve the accuracies of stroke lines, our learning strategy follows the *Greedy Strategy* and *Markov Decision Process*. Specifically, regardless of the previous and future canvas, we only focus on the current canvas and predict the optimal stroke line which makes the next canvas most similar to M .

Basic of model-based DRL: our MARVEL roughly utilizes

the framework of model-based DRL. Compared with model-free DRL methods that sample at will from environments, model-based DRL methods construct dynamics models to simulate the environments as they sample [46]. Leveraging dynamics models for policy updates, the complexity and difficulty of sampling can be reduced significantly. The key to a successful model-based DRL method is to design a suitable policy, state, reward, and dynamics model. Below we detail the design of MARVEL.

Policy: as shown in Figure 4 left, our method follows the policy of model-based Deep Deterministic Policy Gradient (DDPG) [47] that uses the actor-critic architecture [48]. Our architecture consists of two networks, the actor $\pi(s_t)$ and critic $Q(s_t)$. The actor models a policy π that predicts action a_t from state s_t , and the critic estimates the current reward \mathcal{R}_t by

$$Q(s_t) = \mathcal{R}_t(a_t, s_t) + \gamma Q(s_{t+1}), \quad (1)$$

where $\mathcal{R}_t(a_t, s_t)$ is the current reward calculated by a_t and s_t , γ is the discount factor, and the actor $\pi(s_t)$ is trained to maximize $Q(s_t)$ estimated by the critic.

State: our defined state s_t is independent from timestep t , and s_t consists of two parts: the current canvas c_t and the target manga M , represented as $s_t = \{c_t, M\}$. Initializing with a blank canvas c_0 , the actor π predicts action $a_t = \pi(s_t)$ according to t -th state s_t , and the $(t+1)$ -th canvas $c_{t+1} = c_t + \mathcal{D}(a_t)$ is rendered by the drawing module \mathcal{D} , $c_t = c_0 + \sum_{k \in \{0, 1, \dots, t\}} l_k$. Then, the next state s_{t+1} is represented as $s_{t+1} = \{c_t + \mathcal{D}(\pi(s_t)), M\}$.

Drawing module: we design a drawing module \mathcal{D} as the dynamics model of our model-based DRL, and \mathcal{D} is employed to render an action a_t to a stroke line l_t , formulated as $l_t = \mathcal{D}(a_t)$, $a_t \in [0, 1]$. Although training a neural render to map a_t to l_t is flexible (e.g., [49]), it compromises stroke lines' accuracies (e.g., irregular or blurring edges, losing pixels).

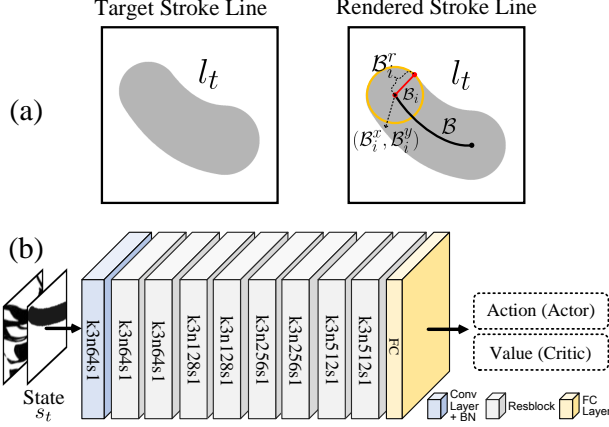


Fig. 5: (a) The detail of drawing module \mathcal{D} to render a stroke line l_t . (b) Network architectures of actor and critic.

Therefore, \mathcal{D} is design by an image rendering algorithm.

As shown in Figure 5(a), the path of l_t is designed to follow the rules of Quadratic Bézier Curve (QBC), and the i -th point B_i on a QBC \mathcal{B} is represented as

$$\begin{aligned} B_i^x &= (1-i)^2 P_0^x + 2(1-i)i P_1^x + i^2 P_2^x \\ B_i^y &= (1-i)^2 P_0^y + 2(1-i)i P_1^y + i^2 P_2^y, \\ B_i^r &= (1-i) P_0^r + i P_2^r \end{aligned} \quad (2)$$

where (B_i^x, B_i^y) and B_i^r indicate the (x, y) coordinates and the radius of B_i respectively, $i \in [0, 1]$. P_0 , P_1 , and P_2 are the three control points of QBC \mathcal{B} .

Action: corresponding to \mathcal{D} , the designed action a_t consists of nine control parameters of a QBC, defined as

$$a_t = (P_0^x, P_0^y, P_1^x, P_1^y, P_2^x, P_2^y, P_0^r, P_2^r, g)_t, \quad (3)$$

where (P_0^x, P_0^y) , (P_1^x, P_1^y) , and (P_2^x, P_2^y) indicate the (x, y) coordinates of P_0 , P_1 , and P_2 respectively. P_0^r and P_2^r control the width of a stroke line, and g controls the color in the 1-channel grayscale space, containing 11 gray levels, i.e., $255 \times \{0, 0.1, 0.2, \dots, 1\}$.

Reward: the basic idea of our designed reward is that in each timestep t , we encourage π to predict the most accurate stroke line l_t which makes the next canvas most similar to M . Huang *et al.* [49] propose that employing the L2 reward \mathcal{R}_{L_2} can train the agent to draw a target image gradually, represented as

$$\mathcal{R}_{L_2} = \|c_t - M\|^2 - \|c_{t+1} - M\|^2, \quad (4)$$

where \mathcal{R}_{L_2} means to encourage the next canvas c_{t+1} to be more similar to M than the current canvas c_t .

However, we observe in experiments that \mathcal{R}_{L_2} typically incur the agent to predict inaccurate stroke lines. First, as shown in Figure 6(a), for targets with strokes in different colors, the agent produces a larger stroke with an average color. Second, as shown in Figure 6(b), for targets with a larger stroke line, the agent will produce numerous smaller strokes repeatedly. Although these two situations also satisfy the increase of \mathcal{R}_{L_2} , the predicted stroke lines are inaccurate

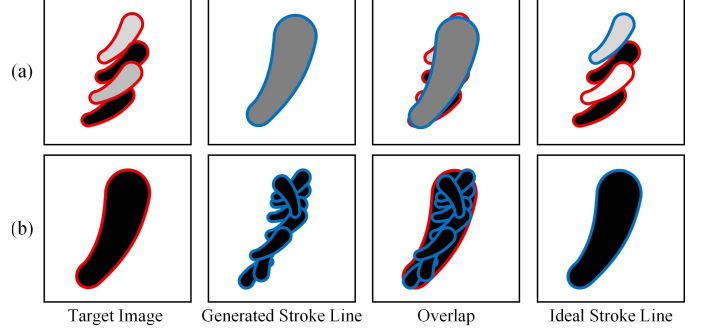


Fig. 6: The baseline reward \mathcal{R}_{L_2} incurs the trained agent to predict inaccurate stroke lines. (a) For a target with strokes in different colors, the agent generates a larger stroke with an average color. (b) For a target with a larger stroke, the agent generates numerous smaller strokes repeatedly. Although these two situations also satisfy the increase of \mathcal{R}_{L_2} , the predicted stroke lines are inaccurate and undesired.

and unideal.

To predict accurate stroke lines, we propose a *Stroke Accuracy* reward \mathcal{R}_t . Let c_t , c_{t+1} , and l_t indicate the current canvas, the next canvas, and the stroke line respectively, $c_{t+1} = c_t + l_t$. We divide l_t into two parts, the stroke area l_t^b and the stroke color $g_t \in [0, 1]$, $l_t = l_t^b \times g_t$. l_t , l_t^b , and c_t have the same shape of $C \times H \times W$. l_t^b is a matrix consisting of 1 and 0, where each entry in the stroke area is set to 1, and other entries are set to 0. Then, our reward \mathcal{R}_t is defined as:

$$\begin{aligned} \mathcal{R}_t &= \lambda_1 r_1^t + \lambda_2 r_2^t + \lambda_3 r_3^t \\ r_1^t(l_t) &= \frac{1}{CHW} \cdot \sum_{(i,j) \in l_t^b} l_t^b(i,j) \\ r_2^t(l_t, c_t, c_{t+1}) &= \frac{1}{CHW} \|l_t^b \times c_t - l_t^b \times c_{t+1}\|^2 \\ r_3^t(l_t, c_{t+1}, M) &= 1 - \frac{1}{CHW} \|l_t^b \times c_{t+1} - l_t^b \times M\|^2 \end{aligned} \quad (5)$$

where λ_1 to λ_3 are used to balance the multiple objectives, (i, j) is an entry in matrix l_t^b , and $\{r_1^t, r_2^t, r_3^t\} \in [0, 1]$. The underlying ideas of the rewards are as follows:

- r_1^t encourages π to maximize the area of generated stroke line l_t .
- r_2^t encourages π to maximize the difference between $l_t^b \times c_t$ and $l_t^b \times c_{t+1}$.
- r_3^t encourages π to maximize the similarity between $l_t^b \times c_t$ and $l_t^b \times M$.

Network architecture: as shown in Figure 5(b), to extract features of manga textures with high complexity, our actor and critic use the residual structure similar to ResNet-18 [50]. The actor utilizes the Batch Normalization [51] and the critic utilizes Weight Normalization [52] with Translated ReLU (TReLU) [31] to stabilize the learning, and all input training images are resized to 128×128 . According to the method of model-based DDPG [49], we utilize the soft target network that constructs a copy for the actor and critic, and updates their weights by making them slowly track the learned networks.

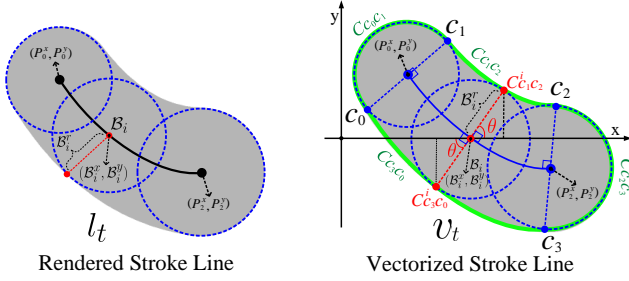


Fig. 7: Design of vectorized stroke line v_t . **Left:** the rendered stroke line l_t . **Right:** the corresponding vectorized stroke line v_t , where v_t and l_t have the same geometry. The key to producing v_t is to fit the QBC representation of the green path C which consists of four curves $C_{c_0c_1}$, $C_{c_1c_2}$, $C_{c_2c_3}$, and $C_{c_3c_0}$.

Algorithm 1: Pruning Algorithm.

Input: \mathcal{V} , M , ξ ;
1 Initialize $\mathcal{V}' = \emptyset$;
2 **for** $\mathcal{V}_p \in \mathcal{V}$ **do**
3 $k \leftarrow |\mathcal{V}_p|$;
4 $t \leftarrow k$;
5 $\delta \leftarrow \frac{\|M_p - R(\mathcal{V}_p)\|_2^2}{C \times H \times W}$;
6 **while** $t > 0$ **do**
7 $\mathcal{V}'_p \leftarrow \mathcal{V}_p$;
8 Remove v_t^p in \mathcal{V}_p ;
9 $\delta' \leftarrow \frac{\|M_p - R(\mathcal{V}'_p)\|_2^2}{C \times H \times W}$;
10 **if** $\delta' \leq \delta + \xi$ **then**
11 $\delta \leftarrow \delta'$;
12 $\mathcal{V}'_p \leftarrow \mathcal{V}'_p$;
13 $t \leftarrow t - 1$;
14 **else**
15 $\mathcal{V}_p \leftarrow \mathcal{V}'_p$;
16 $t \leftarrow t - 1$;
17 **end**
18 **end**
19 Insert \mathcal{V}'_p into \mathcal{V}' ;
20 **end**
Output: \mathcal{V}' ;

C. Vectorization Phase

Figure 4 right shows the pipeline of vectorization phase Ψ_v . First, we divide raster manga M into p patches $M = \{M_0, M_1, \dots, M_p\}$ to adapt to the input size of actor π . Next, utilizing the well-trained π , we predicts an action sequence $\mathcal{A}_p = \pi(M_p) = \{a_0^p, a_1^p, \dots, a_t^p\}$ for each patch p . Then, \mathcal{A}_p is fitted to a sequence of vectorized stroke lines $\mathcal{V}_p = \Phi(\mathcal{A}_p)$ by a fitting module Φ . Finally, the pruning module optimizes \mathcal{V}_p 's file size and accuracy to output the vectorization result $\mathcal{V} = \{\mathcal{V}_0, \mathcal{V}_1, \dots, \mathcal{V}_p\}$.

Action to vectorized stroke line: in fitting module Φ , each action a_t is translated to a vectorized stroke $v_t = \Phi(a_t)$, where v_t and l_t have the same geometry. As shown in Figure 7 right, the key to producing v_t is to fit the QBC representation of the green path C which is composing of four curves $C_{c_0c_1}$, $C_{c_1c_2}$, $C_{c_2c_3}$, and $C_{c_3c_0}$. First, following the definition of a_t in Eq.(3),

$C_{c_0c_1}$ and $C_{c_2c_3}$ can be easily obtained by fitting the arcs of circles whose center coordinates are (P_0^x, P_0^y) and (P_2^x, P_2^y) respectively. Then, let $C_{c_1c_2}^i$ indicates the i -th point on $C_{c_1c_2}$, the x and y coordinates of $C_{c_1c_2}^i$ are computed by

$$C_{c_1c_2}^{i,x} = B_i^x + \cos(\theta) \cdot B_i^r, \quad C_{c_1c_2}^{i,y} = B_i^y + \sin(\theta) \cdot B_i^r, \quad (6)$$

where B_i^x , B_i^y and B_i^r are defined in Eq.(2), $\theta = \arctan[(B_i^y)^{-1}]$, and B_i^r indicates the derivative of B_i . Combining Eq.(2)(3), B_i^r is calculated by

$$B_i^r = \frac{dB_i^y}{dB_i^x} = \frac{(1-i)(P_1^y - P_0^y) + i(P_2^y - P_1^y)}{(1-i)(P_1^x - P_0^x) + i(P_2^x - P_1^x)}. \quad (7)$$

Following Eq.(6) and (7), though fitting the computable points on $C_{c_1c_2}$ and $C_{c_3c_0}$, we can obtain the QBC representations of each curves, and finally fit the path C and the vectorized stroke v_t .

Pruning module: in Ψ_v , there are two issues compromise the performance on vectorization. First, the actor π may produce erroneous strokes that reduce the vectorization accuracy. Second, some repeated or redundant strokes increase the file sizes of vectorized results.

To address these two issues, we propose a pruning module to optimize the erroneous and repeated stroke lines. As shown in Algorithm 1, we input the vectorized result \mathcal{V} of p patches and output the pruned result \mathcal{V}' , where $\mathcal{V} = \{\mathcal{V}_0, \mathcal{V}_1, \dots, \mathcal{V}_p\}$ and $\mathcal{V}_p = \{v_0^p, v_1^p, \dots, v_t^p\}$. M is the target raster manga, and ξ indicates the tolerable error that is used to trade-off the visual similarity and the file size of \mathcal{V}' . In the 3-rd line, $|\mathcal{V}_p|$ indicates the cardinality of \mathcal{V}_p (i.e., the maximum number of stroke lines). In the 5-th line, the function $R(\mathcal{V})$ maps \mathcal{V} to a raster image by CairoSVG [56], and δ is the measured difference between $R(\mathcal{V}_p)$ and M_p . M_p and $R(\mathcal{V}_p)$ have the same shape of $C \times H \times W$.

IV. EXPERIMENT

Below we evaluate the performance of MARVEL in 5 aspects: vectorization accuracy, visual effect, file sizes, time cost, and print quality.

A. Implementation

Dataset: for training MARVEL, we collect a dataset *DeepManga* from several popular manga works. DeepManga contains 42599 raster mangas with different resolutions. In the learning phase, each training data is converted to 1-channel grayscale space, and we randomly cut 128×128 images from original data as the inputs.

Experimental setting: our MARVEL is implemented in PyTorch, and all comparison methods and experiments are performed on a computer with an NVIDIA Geforce RTX 2080 GPU, and 16 Intel(R) i7-10700F CPU. The learning rates of actor (or critic) are from 3×10^{-4} to 1×10^{-4} (or 1×10^{-3} to 3×10^{-4}), which decays after 1×10^5 training batches. We set 1 action per timestep, 40 timesteps per episode, and the reward discount factor is 0.95⁵. In all experiments, by default, we set $\lambda_1, \lambda_2, \lambda_3 = 1$ in Eq.(5), the maximum number of strokes $k = 40$, and the number of patches $p = 32 \times 32$.

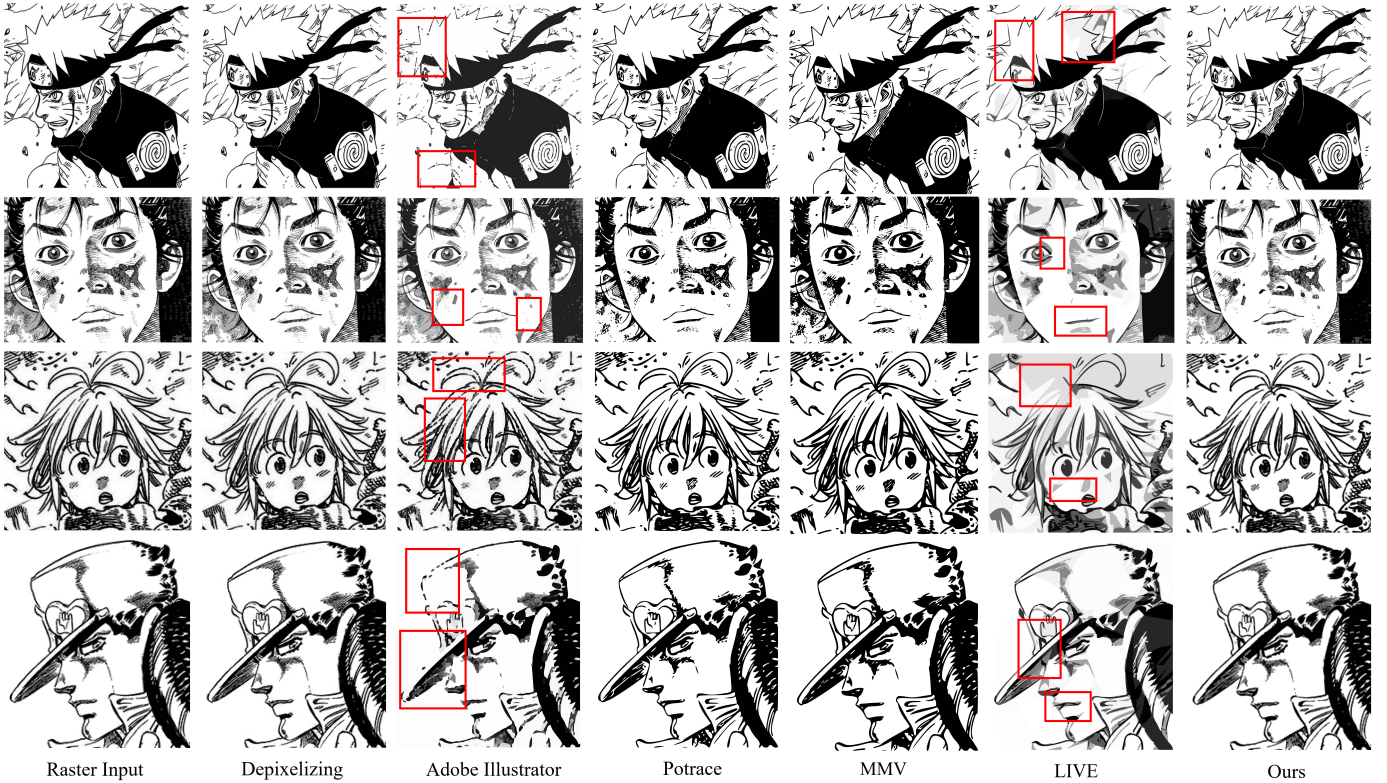


Fig. 8: Comparison with representative methods and commercial packages that can vectorize complex contents, including Depixelizing [4], Adobe Illustrator [53], Potrace [54], MMV [55], and LIVE [26].

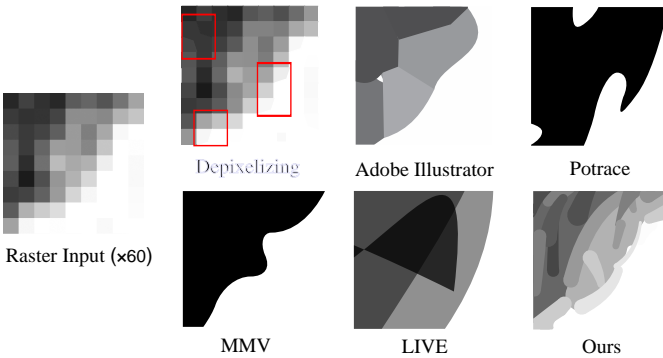


Fig. 9: Enlarged view ($\times 60$) of samples in Figure 8. Although Depixelizing [4] generates accurate vectorized results, the method converts all pixels to square vector grids and only smooths several critical paths, which incurs the results to look as blurry as the raster inputs (red boxes). By contrast, our method achieves a better balance in accuracy and smoothness.

Evaluation index of vectorization accuracy: for evaluating the vectorization accuracy objectively, we leverage indexes *MSE* (Mean Square Error) and *SSIM* [57] (Structural Similarity) to measure the similarities between inputs and outputs. In evaluations, each result in vector space is rasterized to images of size 512×512 by CairoSVG [56]. The MSE index is computed by $\frac{\|I - O\|_2^2}{C \times H \times W \times 255} \in [0, 1]$, where I and O indicate the raster input and the vectorized output of shape $C \times H \times W$. The SSIM index is in $[-1, 1]$, and the index value is proportional

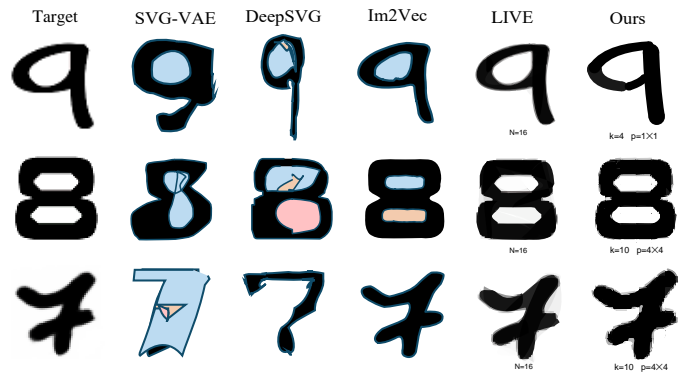


Fig. 10: Comparison with learning-based methods in vectorizing images with simple structures (e.g., FONTS).

to the similarity between two images.

B. Comparison with algorithm-based methods

We first compare our MARVEL with representative methods of algorithm-based vectorization and commercial packages, including Depixelizing [4], Adobe Illustrator [53] (high fidelity mode), Potrace [54], and MMV (Mesh-based Manga Vectorization) [55]. We randomly select 50 raster inputs in Deepmanga, and generate 50 vectorized outputs by each compared method.

Visual perception: the vectorization results of each method are shown in Figure 8 and Figure 9. The outputs of Adobe Illustrator [53] typically lose contents (Figure 8 red boxes) of

TABLE II: Average vectorization accuracies for different manga types, including manga with sparse hatching (SH), dense hatching (DH), solid black strokes (SB), dense screentones (DS), and sparse screentones (SS). **Upper: MSE. Bottom: SSIM.** MMV [55] and Potrace [54] excel at handling black-and-white (binarized) mangas. Especially, MMV is particularly adept at handling screentones. For binarized mangas, MMV, Portace, and Depixelizing [4] achieve the top-3 accuracies. For gray-level mangas, Depixelizing and our approach generate the most accurate results in both visual perception and objective measurement.

Method\Manga type	Binarized GT					Gray-level GT				
	SH	DH	SB	DS	SS	SH	DH	SB	DS	SS
Depixelizing	0.0542	0.0568	0.0538	0.0554	0.0588	0.0702	0.0682	0.0713	0.0696	0.0722
Adobe	0.1184	0.1365	0.1042	0.1285	0.1162	0.1367	0.1402	0.1338	0.1398	0.1323
Potrace	0.0819	0.0813	0.0815	0.0843	0.0825	0.1145	0.1253	0.0933	0.1135	0.1205
MMV	0.0765	0.0804	0.0753	0.0795	0.0778	0.0883	0.0979	0.0865	0.0845	0.0838
Ours	0.0826	0.0858	0.0825	0.0848	0.0834	0.0812	0.0863	0.0794	0.0837	0.0826
Depixelizing	0.9554	0.9425	0.9607	0.9405	0.9372	0.9532	0.9573	0.9405	0.9513	0.9472
Adobe	0.6203	0.5826	0.6312	0.5925	0.6275	0.6407	0.6152	0.6530	0.6223	0.6512
Potrace	0.9327	0.8896	0.9354	0.9180	0.9212	0.8241	0.7685	0.9075	0.8364	0.8417
MMV	0.9415	0.8965	0.9442	0.9342	0.9435	0.8532	0.7913	0.9205	0.8605	0.8741
Ours	0.9231	0.8670	0.9252	0.8724	0.9193	0.9352	0.8750	0.9261	0.8873	0.9025

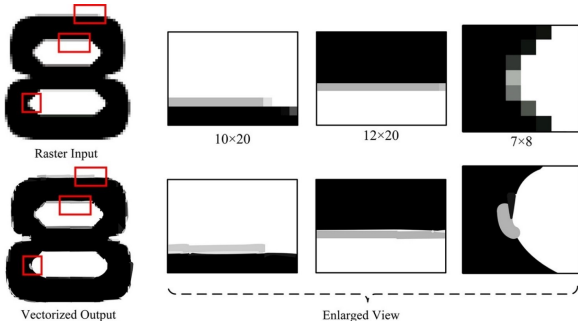


Fig. 11: The vectorized gray regions (red boxes) are generated intentionally, which aims to accurately follow the gray pixels (red boxes) in raster inputs.

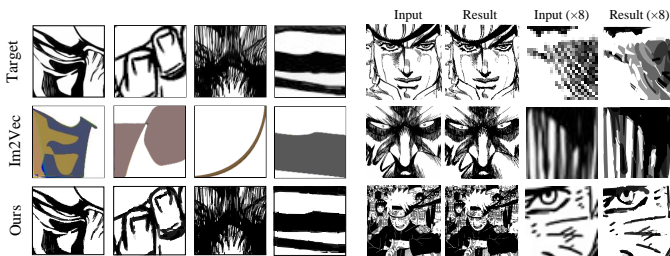


Fig. 12: **Left:** comparison with Im2Vec [13] that can be trained without vector supervised. **Right:** our vectorized results at different scales.

inputs. Potrace [54] neither handles multiple colors nor preserves accurate pixel details. MMV [55] excels at vectorizing screentones, yet, for complex input manga without screentones, MMV typically produces binary colors and ignores gray regions, which reduces the vectorization accuracy. In Section IV-D, we detaily summarize the advantages and disadvantages of MMV.

In addition, the algorithm-based methods need to design tailored algorithms for different scenarios, which typically

include complex image segmentation and curve-fitting. Our method aims to train an end-to-end neural model that can replace the algorithm design, image segmentation, and curve fitting.

Accuracies of vectorizing different manga types: for a fair comparison, first, we divide our test data into five manga categories, including manga with sparse hatching (SH), dense hatching (DH), solid black strokes (SB), dense screentones (DS), and sparse screentones (SS). Next, each ground truth (GT) is processed into two types, that is, binarized GT G^b and multi-gray levels GT G^g . Then, we vectorize G^b and G^g by each algorithm-based method, respectively.

The average vectorization accuracies are summarized in Table II. We observe that MMV [55] and Potrace [54] excel at handling black-and-white (binarized) mangas. Especially, MMV is particularly adept at handling screentones. For binarized mangas, MMV, Portace, and Depixelizing [4] achieve the top-3 accuracies. For multi-gray level manga, Depixelizing [4] and our approach generate the most accurate results in both visual perception and objective measurement. Yet, Depixelizing converts pixels to square vector grids and only smooths several critical paths, which incurs the vectorization results to look as blurry as the raster inputs when zooming in (red boxes in Figure 9). By contrast, our MARVEL achieves a better balance between accuracy and smoothness.

C. Comparison with learning-based methods

Next, we compare our MARVEL with representative learning-based vectorization methods, including SVG-VAE [29], DeepSVG [30], Im2Vec [13], and LIVE [26] (N=256).

Vectorization on simple structures: we compare the vectorization accuracies on datasets with simple image structures (e.g., FONTS). Figure 10 and Table III show the comparison results in visual perception and objective indexes respectively.

Compared with other learning-based methods, our vectorization results have high accuracies in objective and subjective,

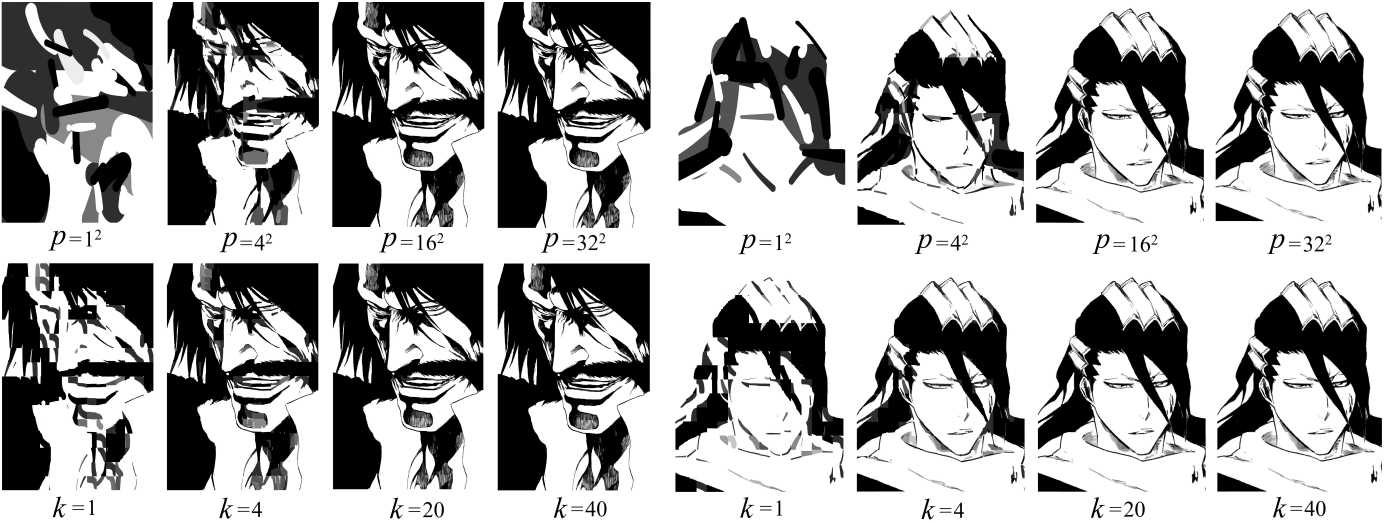


Fig. 13: Our vectorized results under different settings of p and k . **Upper:** influence of p , when $k = 40$. **Bottom:** influence of k , when $p = 16^2$. Our vectorization accuracies are increasing with p and k through subjective visual perception, and the objective evaluation is shown in Figure 14.

TABLE III: Average vectorization accuracies compared with learning-based methods.

Index	MSE		SSIM	
	FontS	DeepManga	FontS	DeepManga
Method\Dataset	FontS	DeepManga	FontS	DeepManga
SVG-VAE	0.3815	×	0.4328	×
DeepSVG	0.3433	×	0.5238	×
Im2Vec	0.0532	0.2445	0.8083	0.3879
LIVE	0.0293	0.1672	0.8852	0.6787
Ours	0.0261	0.0825	0.9303	0.8968

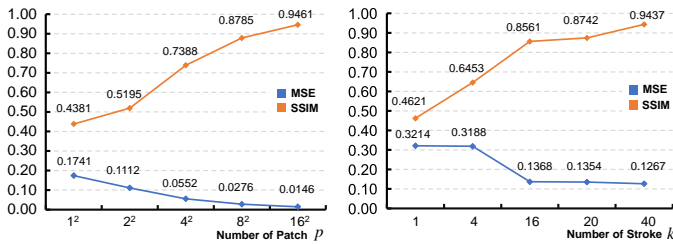


Fig. 14: Average vectorization accuracies in 100 random samples, under different settings of p and k . The accuracies are proportional to p and k , and the growth rates of accuracies are decreased when k is higher than a threshold (i.e., $k \geq 16$)

and reaches the state-of-the-art level for vectorizing images with simple structures. Moreover, as shown in Figure 11, the artifacts-like vectorized gray regions (red boxes) are generated intentionally, which aims to accurately follow the gray pixels (red boxes) in raster inputs. This phenomenon is caused by unclear pixel outlines in raster inputs, and then our method will consider these unclear pixels as the vectorization targets, when setting a large p to increase the detail level.

Vectorization on complex structures: utilizing 50 random cropped inputs of sizes 128×128 in Deepmanga, we

TABLE IV: Differences between our approach and state-of-the-art learning-based vectorization methods (i.e., SVG-VAE [29], DeepSVG [30], Im2Vec [13], and LIVE [26]).

Performance\Method	SVG-VAE	DeepSVG	Im2Vec	LIVE	Ours
Vectorize simple texture	✓	✓	✓	✓	✓
Vectorize complex texture	✗	✗	✗	✓	✓
W/O vector supervision	✗	✗	✓	✓	✓
Average time cost	1.12s	0.05s	14.37s	25.88h	48.23s

compare the performance of vectorizing complex structures. We only compare our method with Im2Vec [13] (trained by dataset DeepManga) and LIVE [26], since DeepSVG [30] and SVG-VAE [29] cannot be trained without the vector supervision. Moreover, Reddy et al. [13] have proved that Im2Vec outperforms DeepSVG and SVG-VAE on vectorization accuracies.

Comparison results are shown in Figure 9, Figure 12 and Table III. Im2Vec cannot handle target with complex content, and LIVE (N=256) may miss the contents of inputs and produces gray outputs from white targets (Figure 8 red boxes). In addition, LIVE is an iteration-based method that optimizes each vector element using 500 iterations (1-5 seconds per iteration, increasing with the indexes of vector elements), which takes an average of 25.88 hours to vectorize one image, when setting N=256 and N indicates the maximum number of vector elements.

To summarize, as shown in Table IV, first, our method outperforms compared learning-based methods in the accuracies of vectorizing simple and complex structures. Second, our method has the merit that only needs supervision from raster images without high-cost vector annotation. Third, compared with LIVE [26] which can vectorize complex contents (average 25.88 hours when N=256), our method takes much less

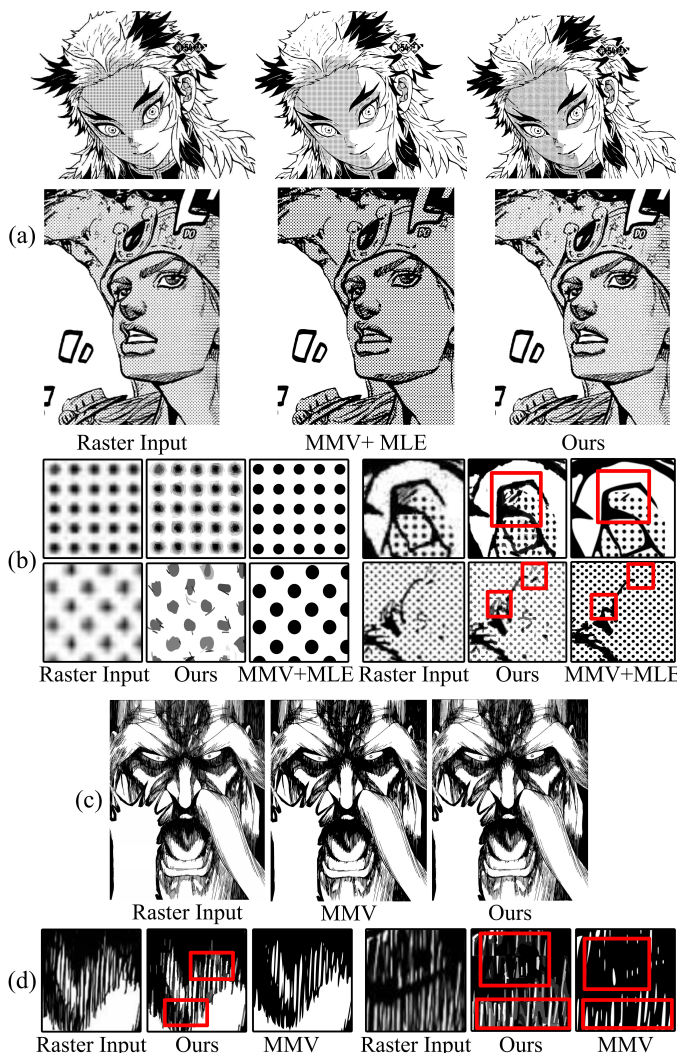


Fig. 15: Comparison with MMV [55]. (a) Vectorization of manga with screentones [36]. (b) Enlarged view of (a). (c) Vectorization of manga with complex structures (e.g., dense hand-drawing shadows). (d) enlarged view of (b).

time (average 48.23 seconds when $p=16^2$, $k=20$)¹.

D. Comparison with manga and line-art vectorization methods

Manga vectorization: as shown in Figure 15, we first compare and discuss our performance with manga vectorization method MMV [55]. In implementing MMV, we adopt MLE (Manga Line Extraction [34]) instead of the original screentones detection method. MMV offers some benefits, including the ability to extract key vector paths for easy shape editing and smaller file sizes (averaging 126.35KB), and MMV excels at handling screentones [Figure 15(a)(b)]. However, it has some limitations. First, as shown in Figure 15(d), MMV sacrifices performance in preserving similarities (Table II) and color levels (i.e., only preserves binary colors except for screentones while ignoring gray regions). Second,

¹Detailed evaluation of our time-cost is shown in Section IV-G.

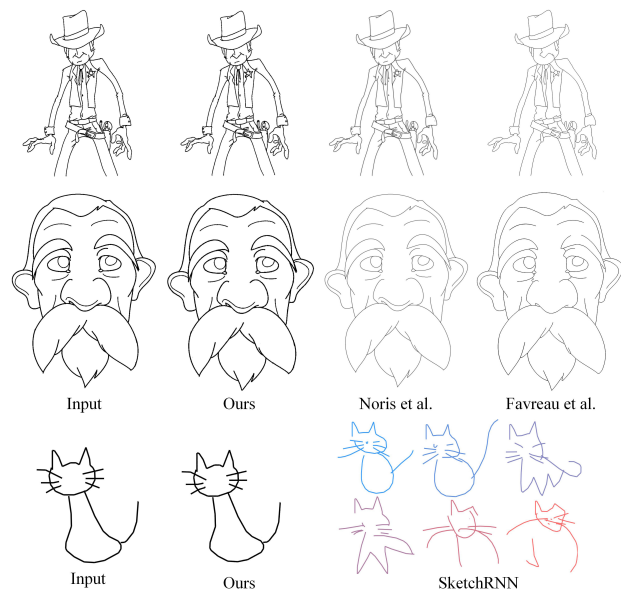


Fig. 16: Comparison with representative line-art vectorization methods, including Noris et al. [6], Favreau et al. [58], and SketchRNN [27].

it struggles to preserve complex structures (e.g., dense hand-drawing shadow lines [Figure 15(d) red boxes]), which may lose some contents and stroke lines [Figure 15(b) red boxes]. By contrast, our advantages are as follows. First, we preserve high similarities and color levels with input mangas. Second, our method excels at handling complex manga structures. Nevertheless, our method has two limitations. First, it cannot extract key paths, resulting in larger file sizes (averaging 734.54KB). Second, it lacks a dedicated setting to process manage screentones.

Line-art vectorization: we next compare and discuss our method with representative line-art vectorization methods, including Noris et al. [6], Favreau et al. [58], and SketchRNN [27]. As shown in Figure 16 and Figure 17, these methods are typically employed to extract the vector centerline of the line-art drawings (e.g., sketches, clean line drawings). SketchRNN [27] reconstructs vector paths according to the input sketches, and outputs a series of vectorized results with similar structures and paths. By contrast, our method aims to preserve high similarities with inputs and cannot simplify contents to key paths.

E. Ablation study

Influence of patches and strokes: in MARVEL, there are two manners to increase the vectorization accuracy while compromising the time cost. First, dividing a target image into small patches and vectorizing each of them. Second, increasing the maximum number of stroke lines. Accordingly, we conduct an experiment to evaluate the influence of the number of patches p and the maximum number of stroke lines k .

In Figure 13, we display our vectorized results under different settings of p and k , and the average vectorization accuracies in 100 random samples are shown in Figure 14. When setting a small p , the dense textures may be vectorized



Fig. 17: Comparison with Noris et al. [6] for vectorizing line-art and complex mangas.

as a rough gray region to decrease the file size. When setting a large p , the textures or strokes in vectorized results are obvious and clean. Our vectorization accuracies are proportional to p and k , and the growth rates of accuracies are decreased when k is higher than a threshold (i.e., $k \geq 16$). Empirically, setting $p=16 \times 16$ and $k=20$ is enough to produce results with high accuracies.

Influence of rewards setting: to evaluate our rewards' effectiveness in improving accuracies, we train a DRL agent leveraging each of \mathcal{R}_{L2} (baseline [49]), $(r_2 + r_3)$, $(r_1 + r_3)$, $(r_1 + r_2)$, and $(r_1 + r_2 + r_3)$ respectively. As shown in Figure 18, the visual comparison demonstrates that without r_1 , the agent tends to predict small and inaccuracy strokes. Without r_2 , the differences between the current and next canvas are decreased, which incurs the overlap of strokes (marked with red boxes). Without r_3 , the combination of strokes cannot progressively be similar to the ground truth. The scatter and box charts in Figure 19 display the measured similarities between inputs and outputs in 100 random samples when $k=40$ and $p=1 \times 1$, which also shows our proposed rewards can effectively improve the accuracy of stroke lines. To sum up, each term of our proposed rewards is effective to predict more accurate strokes in each timestep, and significantly outperforms the baseline.

F. User study:

Below we conduct two user studies to subjectively evaluate our results' visual effects and accuracies, and 20 volunteers are invited to participate in the studies.

Comparison with related methods: after observing 20 samples produced by each compared method, all volunteers are asked to vote for the two methods whose results are most visual-pleasant and most accurate respectively. The study results in Figure 20 indicate that on average, 3.75 (18.75%) and 4.00 (20.00%) volunteers believe our results have the highest visual quality and accuracy respectively. Table V shows the

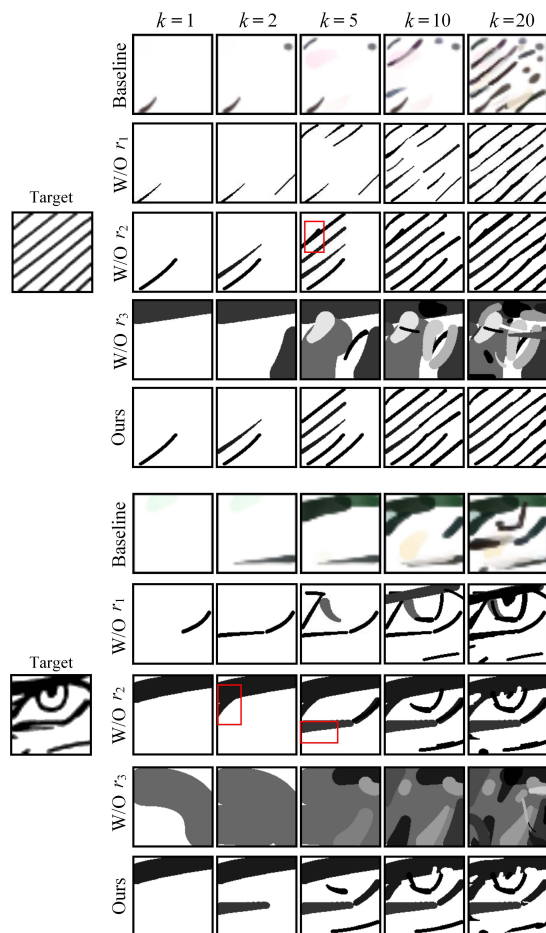


Fig. 18: Ablation study of rewards settings, including \mathcal{R}_{L2} reward (baseline [49]), and results without r_1 , r_2 , and r_3 respectively. Objective comparison is shown in Figure 19.

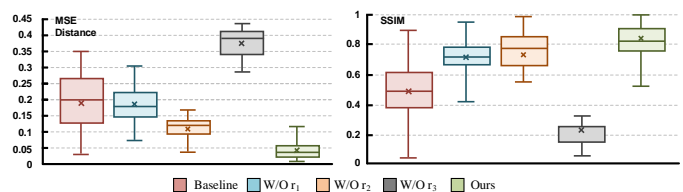


Fig. 19: Object similarities between inputs and outputs in 100 random samples when $k=20$ and $p=1 \times 1$.

paired two-tailed t-test of our user studies in Figure 20, where \bar{X} , S , and D indicate mean, standard deviation, and difference of mean, respectively. To sum up, compared with algorithm-based and learning-based methods, our approach achieves state-of-the-art performance on visual effect and vectorization accuracy.

Subjective perception of visual effect and accuracy: another user study is to evaluate the subjective perception of our approach in visual effect and accuracy. First, we randomly generate 20 paired samples containing raster inputs and corresponding vectorized outputs. Then, the samples are displayed on a webpage, and 20 volunteers are invited to finish two tasks after observation. The first task is to vote for the satisfaction levels of visual effect, and another task is to vote

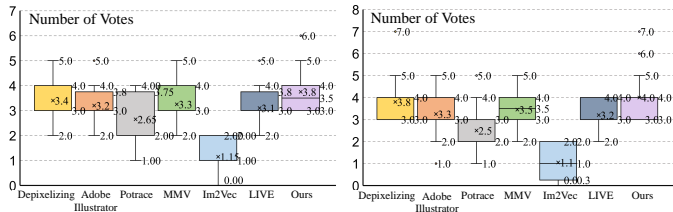


Fig. 20: Comparison with related methods in manga vectorization. **Left:** voting results for visual effect. **Right:** voting results for vectorization accuracy.

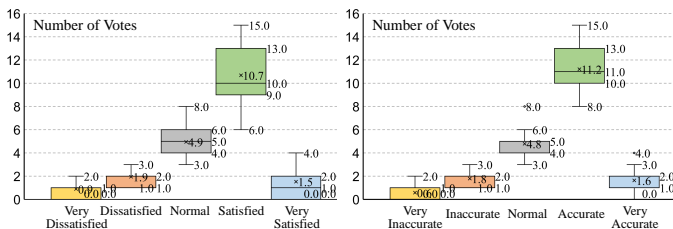


Fig. 21: User studies on visual effect and vectorization accuracy of our results. **Left:** voting results for visual effect. **Right:** voting results for vectorization accuracy.

for the accuracy levels.

As shown in Figure 21, for visual effect, 10.68/4.97 (53.42%/24.85%) volunteers on average have voted for the satisfied/normal levels. For accuracy, 11.21/4.79 (56.05%/23.95%) volunteers on average have voted for the accuracy/normal levels. Accordingly, the study results show that our vectorized results satisfy the requirements of most users in visual effect and accuracy.

G. File Size and Time Cost

File size: in MARVEL, the pruning mechanism (PM) is designed to reduce the file sizes of vectorized outputs. To evaluate the effectiveness of PM, we randomly collect 50 raster inputs and generate 100 vectored samples under different settings of p and k . Next, we measure the performance of PM in two aspects, the reduced file sizes and the influences on visual similarity. As shown in Figure 22, the PM effectively reduces the file sizes by an average of 50.53% when $k = 40$. Moreover, the observed results show that the reduced file sizes are proportional to k , since the produced repeated and erroneous strokes are increasing with k and are pruned by PM.

In Figure 23, we display the measured average visual similarities between raster input and vectorized outputs, when $p = 32 \times 32$ and $k = 40$. The scatter and box charts show that the pruning mechanism can preserve and even improve the visual similarity when reducing file sizes, since the mechanism removes the error stroke lines. To summarize, the proposed PM significantly reduces the file sizes of vectorized results without compromising the visual similarity.

Time cost: we evaluate the time costs of our vectorization without PM (only DRL processing) and the time costs of the PM processing. Under different settings of p and k , the

TABLE V: Paired two-tailed t-test of our user studies. **Upper:** voting results for visual effect. **Bottom:** voting results for vectorization accuracy.

Method	$\bar{X} \pm S$	D	t	p
Depixelizing	3.40 ± 0.68	-0.35	-1.277	0.217
Adobe Illustrator	3.20 ± 0.70	-0.55	-1.868	0.077
Potrace	2.65 ± 0.93	-1.10	-3.240	0.004
MMV	3.25 ± 0.72	-0.50	-2.032	0.056
Im2Vec	1.15 ± 0.75	-2.60	-9.133	<0.001
LIVE	3.10 ± 0.79	-0.65	-2.668	0.015
Ours	3.75 ± 0.91	0.00		

Depixelizing	3.80 ± 1.01	-0.20	-0.535	0.599
Adobe Illustrator	3.25 ± 1.02	-0.75	-1.861	0.078
Potrace	2.50 ± 0.89	-1.50	-4.177	0.001
MMV	3.45 ± 0.76	-0.55	-1.764	0.094
Im2Vec	1.05 ± 0.76	-2.95	-9.460	<0.001
LIVE	3.20 ± 0.62	-0.80	-3.559	0.002
Ours	4.00 ± 1.08	0.00		

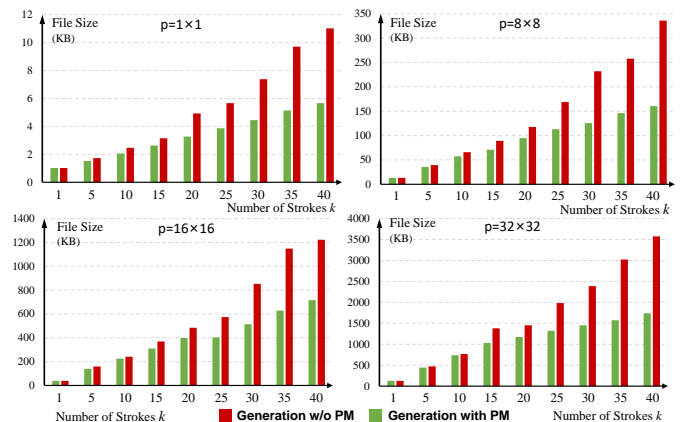


Fig. 22: Influences of the pruning module (PM) on file sizes, under different settings of p and k . The use of PM significantly reduces file sizes, and the reduced file sizes are proportional to k since the produced redundant and erroneous strokes are increasing with k .

calculated average time costs (in seconds) are shown in Table VI, which shows that our time costs are increasing with p and k , and the maximum vectorization time is the acceptable few minutes. Empirically, under the condition of using PM, setting $\{p = 16^2, k = 20\}$ is enough to produce results with high accuracy (average 81.91 seconds), and setting $\{p = 32^2, k = 20\}$ can further vectorize mangas with extremely complex structures (average 153.97 seconds). The above time costs are computed in single-thread mode, and using the multithreading mode can further save the run time.

Memory usage and rendering time: we evaluate the memory usage and render time of our results on different devices. The average test results of 100 random samples are shown in Table VIII. Experimental results show that our results are within an acceptable range in terms of render time and memory usage in various computers and mobile devices,

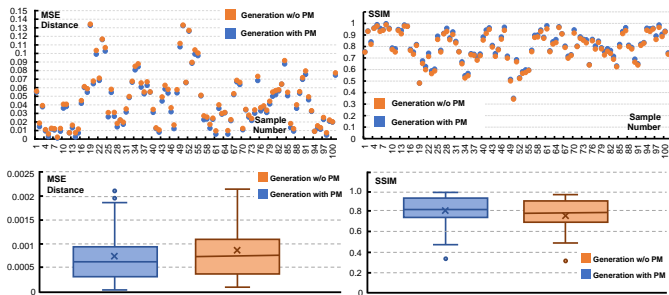


Fig. 23: Objective evaluation of average similarity of 100 paired samples (generation with PM and without PM), when $p = 32^2$ and $k = 40$. The results demonstrate that using PM does not compromise the visual similarity.

TABLE VI: Time costs (in seconds) under different settings of p and k . **Upper:** time costs of vectorization w/o PM. **Bottom:** time costs of PM processing.

$p \setminus k$	1	5	10	15	20	25	30	35	40
1^2	1.22	1.28	1.31	1.35	1.39	1.45	1.50	1.54	1.58
4^2	1.37	1.74	2.22	2.70	3.19	3.67	4.06	4.51	4.97
8^2	1.72	3.43	5.18	7.18	8.91	10.72	12.54	14.35	16.96
12^2	2.45	6.59	12.36	16.32	21.84	26.34	29.12	34.12	37.43
16^2	3.34	10.11	18.15	23.62	33.68	39.24	49.46	53.24	68.60
20^2	4.65	13.25	27.46	37.58	52.63	63.24	76.67	83.14	92.32
24^2	5.92	21.62	39.65	55.28	75.68	91.35	109.43	113.43	118.53
28^2	7.46	28.12	52.38	83.03	102.71	134.62	150.87	189.41	201.99
32^2	9.36	35.89	69.81	98.60	116.35	148.35	185.65	225.32	257.34

$p \setminus k$	1	5	10	15	20	25	30	35	40
1^2	0.02	0.08	0.18	0.22	0.47	0.8	1.08	1.22	2.33
4^2	0.18	0.61	1.54	2.75	5.18	7.82	12.76	18.12	26.53
8^2	0.58	2.11	5.32	10.98	18.95	32.34	49.56	71.31	97.61
12^2	1.53	7.18	12.34	22.98	34.17	50.37	69.25	95.34	189.18
16^2	2.94	11.75	20.48	31.63	48.23	93.24	123.85	165.76	323.71
20^2	4.94	20.13	33.53	64.55	101.34	143.71	198.35	256.37	358.35
24^2	8.31	28.74	46.08	92.96	144.79	203.84	283.63	372.54	517.37
28^2	12.83	34.97	69.77	125.74	197.36	279.56	387.19	503.87	697.64
32^2	20.23	51.54	98.14	165.25	257.23	367.95	506.45	658.32	921.61

which can satisfy different usage scenarios.

H. Evaluation of vectorizing images with different resolutions

We conduct experiments to evaluate our performance in visual effects, file sizes, and accuracies, when vectorizing mangas with different resolutions.

Visual perception and screentone: we evaluate our vectorized results of input mangas with different resolutions. As shown in Figure 24 and Figure 26, for a target manga, we first resize it to different resolutions by CSI (cubic spline interpolation [59]), and then generate the corresponding vectorized results ($p=16^2$, $k=20$). We can observe that our method produces blurry manga screentones in low image resolution, since our goal is to make results similar to the input mangas, and it is a limitation of our method that cannot

TABLE VII: Average vectorization accuracy at different resolutions.

Index \ Resolution		1024×1448	768×1087	512×724	256×362
D_{img}	MSE	0.0000	0.0242	0.0929	0.1410
	SSIM	1.0000	0.9807	0.9170	0.6897
D_{vec}	MSE	0.0813	0.0826	0.1232	0.1804
	SSIM	0.9252	0.8842	0.7693	0.5978

reconstruct manga screentones. Therefore, for reconstructing screentones, MMV [55] performs better than our method.

File size: Figure 25 shows the average file sizes between input images and our vectorized results, under different input resolutions. Each shown file size is the average result computed by 50 random cases, and each image is in PNG format. Combined with Figure 22, we observe that the resolutions of input images do not influence the sizes of our vectorized results which are mainly influenced by the numbers of generated strokes k and patches p . Our method can save file sizes when setting $p = 32^2$ and $k = 20$ for high accuracy (saved about 21.4% file size when input resolutions are 1024×1448), and $p = 16^2$ and $k = 20$ for common accuracy (saved about 59.3% file sizes when input resolutions are 768×1087). Moreover, for input images with low resolution (e.g., 256×362), we can further set smaller p and k to reduce vectorized file sizes.

Vectorization accuracy: first, we randomly select 50 A4 pages of high-resolution input mangas (normalized to 1024×1448). Let M_0 indicate the original high-resolution input manga, we downsample M_0 to M_1 (768×1087), M_2 (512×724), and M_3 (256×362) by CSI [59], respectively. Then, we vectorize $\{M_0, M_1, M_2, M_3\}$ to $\{V_0, V_1, V_2, V_3\}$ ($p=32^2$, $k=20$), and conduct two evaluations D_{img} and D_{vec} . In D_{img} (or D_{vec}), we measure differences between M_0 and M_δ (or differences between M_0 and $\mathcal{R}(V_\delta)$), where $\delta \in \{0, 1, 2, 3\}$, and the function $\mathcal{R}(V_\delta)$ is utilized to rasterize V_δ to images by CairoSVG [56].

The average results are summarized in Table VII, and some magnification examples are shown in Figure 24 and Figure 26. We observe that our vectorization accuracies between $\mathcal{R}(V_\delta)$ and M_0 are directly proportional to the similarities between M_δ and M_0 . Since our method aims to preserve high accuracy between inputs and outputs, thus our method cannot reconstruct high-resolution images by vectorizing the downsampled low-resolution images.

I. Evaluation of Print version

To evaluate our vectorized results' quality in the print version, we select 20 paired samples (raster inputs and vectorized outputs) with extremely complex textures. Next, each sample is printed on A4 paper ($210 \text{ mm} \times 297 \text{ mm}$) and then scanned. The printer and scanner used in experiments is HP LaserJet M1535dnf MFP.

Figure 2 and Figure 27 show the scan results of print versions. By contrast, our vectorized results significantly preserve the visual details of raster inputs, even in the enlarged view. In addition, the colors and lines of our vectorized outputs are even cleaner than raster inputs, since some indistinct and irregular

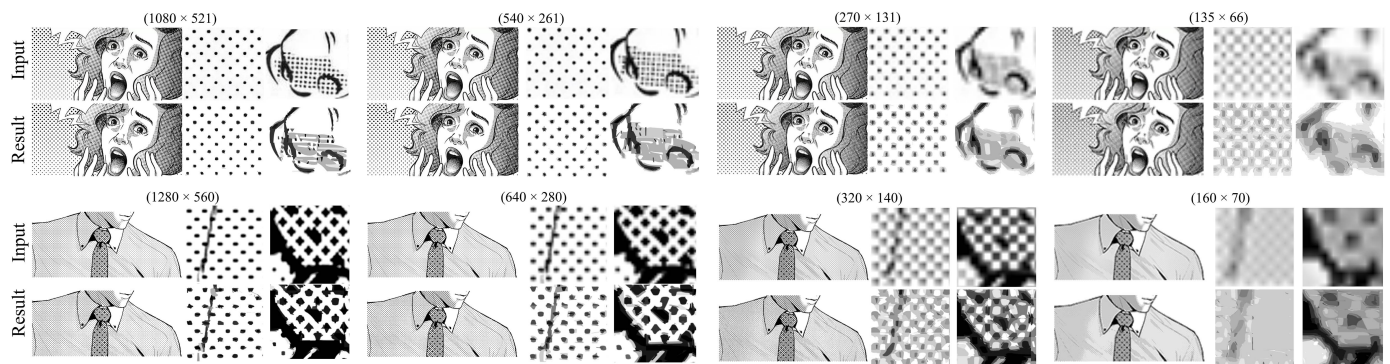


Fig. 24: Vectorized screentones of input images with different resolutions.

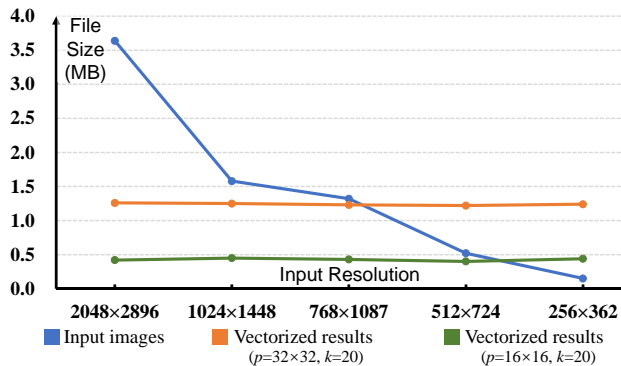


Fig. 25: Evaluation of reduced file sizes between input images and our vectorized results, under different input resolutions. Combined with Figure 22, the input image resolutions do not influence our vectorized file sizes which are mainly influenced by the numbers of generated strokes k and patches p . For input images with low resolution (e.g., 256×362), we can further set smaller p and k to reduce vectorized file sizes.

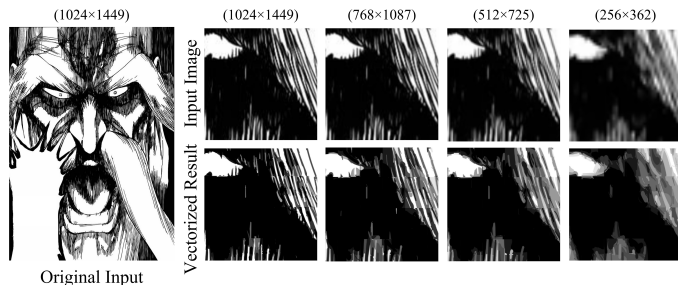


Fig. 26: Enlarged view of vectorized results of input images with different resolutions. The objective measurement results are summarized in Table VII.

pixels (e.g., artifacts in red boxes of Figure 27) will be filtered when our model predicts stroke lines.

V. DISCUSSION AND LIMITATIONS

A. Discussion

Machine learning of manga strokes: the previous literature MMV [55] proposes a stroke-based concept for future work that develops a machine-learning mechanism to automatically add extra manga strokes after deformation. Our work is

TABLE VIII: Memory usage and rendering time of our vectorized results under different situations.

Device	Operating System	PDF Reader	File Size	Memory Usage	Render Time	
Mobile Phone	Iphone 12	IOS	648.38KB ($p = 16^2$, $k = 40$)	Chrome	-	0.52s
				Adobe Acrobat	-	0.44s
				Foxit Reader	-	0.63s
	HUAWEI Mate 40	EMUI/Android		Chrome	-	0.48s
				Adobe Acrobat	-	0.65s
				Foxit Reader	-	0.55s
Computer	Dell Alienware m17R5	Windows	Chrome	11.3MB	0.45s	
			Adobe Acrobat	28.4MB	0.65s	
			Foxit Reader	21.3MB	0.58s	
	Mac book	IOS	Chrome	10.9MB	0.42s	
			Adobe Acrobat	27.9MB	0.53s	
			Foxit Reader	11.2MB	0.56s	

similar to the stroke-based concept proposed by MMV [55]. By comparison, our method is implemented by a tailored deep reinforcement learning framework, and further proposes an accuracy-oriented reward function and action model of construct stroke lines. In addition, we decompose an entire image into strokes, rather than extracting extra strokes

Screentones: screentone [36] is a technique for applying textures and shades to manga, used as an alternative to hatching. In our method, we vectorize a screentone region like vectorizing a general pixel region. Specifically, as shown in Figure 28, the parameter p controls the detail level of our vectorized outputs. When p is large (e.g., $p = 32^2$), the textures and dots in screentones are obvious and clean. When p is small (e.g., $p < 8$), screentones will be vectorized to a region with an average color.

Usage scenario: our vectorization method can translate raster mangas to vector graphics with preserving high similarities in both electric and print versions. Moreover, for showing high-resolution contents, the vectorized mangas have smaller file sizes than raster images. Hence, our method can be applied to store raster mangas in a resolution-independent manner,

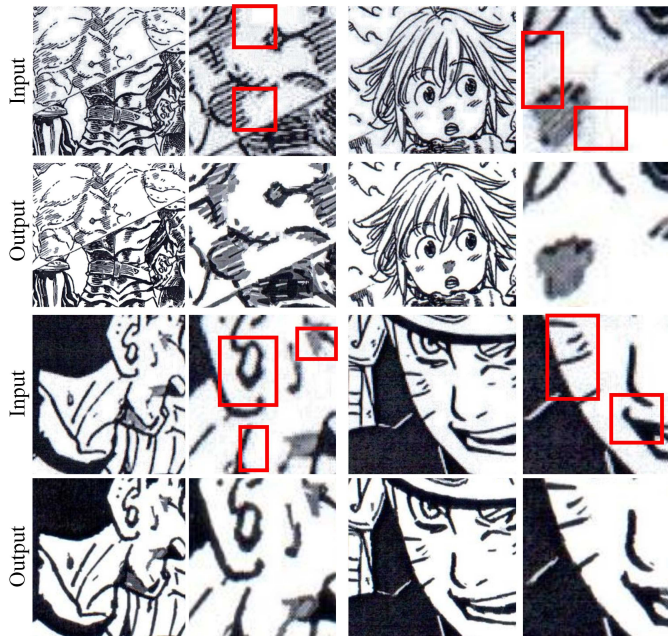


Fig. 27: Scan results of print versions in the enlarged view. By contrast, our vectorized outputs have cleaner colors and lines than raster inputs (red boxes), since indistinct and irregular pixels will be filtered when our model predicts stroke lines.

which is readily displayed on digital devices with different resolutions.

In addition, besides our current usage scenarios, our work presents an enlightening contribution to the application and research of learning-based vectorization. Specifically, in our current method, our vectorized results are composed of many vector primitives based on Bézier curves (as shown in Figure 7), which limits our performance in shape retrieval and content editing. In our future work, we will explore an algorithm that merges two Bézier primitives into one primitive in each step, to extract total vector paths. Then, our method can be applied to the same scenarios (e.g., shape retrieval, content editing) as other vectorization methods (algorithm-based or learning-based).

Processable vector parameter: for the learning-based methods we have compared, Im2Vec [13], SVG-VAE [29], and DeepSVG [30] vectorize an entire image in a one-step manner that limits the number of predictable vector parameters (i.e., several Bézier curves). In addition, LIVE [26] is a special learning-based method that fits curves in a stepwise manner using a neural optimizer without training any model, but the method requires hundreds of iterations to fit each vector curve. By contrast, our method combines the merits of learning-based and stepwise methods, which not only adopts the trained model to fast predict strokes, but also constructs a DRL framework that can infinitely add stroke lines to correct inaccurate areas in a stepwise manner.

Patch Segmentation: MARVEL first segments a raster image into small patches and then vectorizes each patch, and this manner has two advantages. First, it allows and benefits

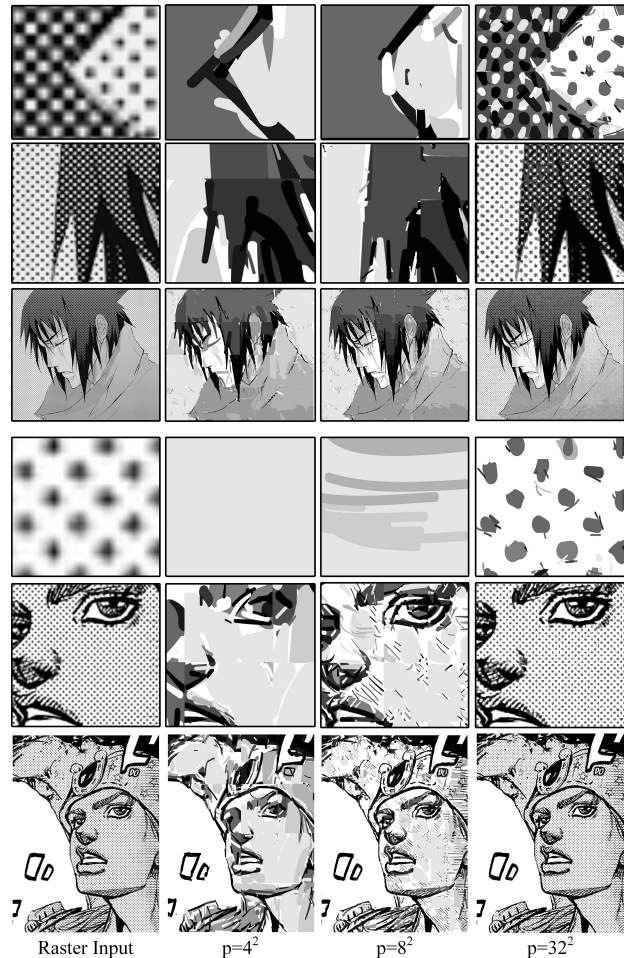


Fig. 28: Vectorized results and enlarged views of manga screentones under different settings of p , when $k=20$.

users to control the levels of vectorization detail. Second, the hundreds of patches can be considered as one input batch of the trained model. Then, the model can vectorize all images in the input batch simultaneously, which significantly increases the vectorization speed. There may be introduced some boundary artifacts, but these artifacts are almost ignorable when setting a large p .

B. Limitation

Visual effect in different readers: as shown in Figure 29, our results may be rendered visually unpleasant by some PDF readers (e.g., SumatraPDF), which causes white gaps among square patches (marked in red boxes). This issue can be solved by zooming in or utilizing other PDF readers (e.g., Chrome, Foxit Reader), and these different rendering effects will not affect the visual quality of the printed version as shown in Figure 2.

Shape editing: our MARVEL is a primitive-based method that represents the global vector graphic as a collection of vector primitives. This is much different from other methods that mainly predict some key vector paths (e.g., [13], [29],

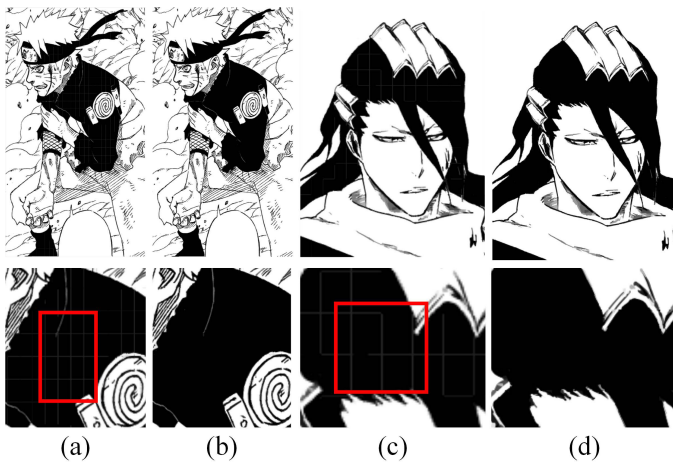


Fig. 29: Screenshots of our results in different PDF readers. (a)(c) Screenshots in SumatraPDF. (b)(d) Screenshots in Chrome. Our results may be rendered visually unpleasant by some PDF readers (e.g., SumatraPDF) which incurs white gaps among square patches (red boxes). This issue can be solved by zooming in or utilizing other PDF readers (e.g., Chrome, Foxit Reader), and these different rendering effects will not affect the visual quality of the printed version.

[30], [60], [61]), and thus our method is not convenient in shape editing.

VI. CONCLUSION

In this paper, we propose MARVEL, a primitive-wise approach for vectorizing raster mangas by DRL. MARVEL introduces a novel perspective that regards an entire manga as a collection of primitives—stroke lines that can be decomposed from the target image for achieving accurate vectorization. Extensive subjective and objective experiments have proved the effectiveness of our improvements, and have shown that compared with both algorithm-based and learning-based methods, our MARVEL can produce impressive results and has reached the state-of-the-art level.

In the future, we aim to explore a sliding window mechanism to avoid the isolation of patches, and explore a stroke fusion mechanism to obtain key paths for achieving convenient shape editing.

REFERENCES

- [1] Z.-Y. Zhu, S. Zhang, S.-C. Chan, and H.-Y. Shum, “Object-based rendering and 3-d reconstruction using a moveable image-based system,” *IEEE Transactions on Circuits and Systems for Video Technology (TCSVT)*, vol. 22, no. 10, pp. 1405–1419, 2012.
- [2] A. Orzan, A. Bousseau, H. Winnemöller, P. Barla, J. Thollot, and D. Salesin, “Diffusion curves: a vector representation for smooth-shaded images,” *ACM Transactions on Graphics (TOG)*, vol. 27, no. 3, pp. 1–8, 2008.
- [3] S.-H. Zhang, T. Chen, Y.-F. Zhang, S.-M. Hu, and R. R. Martin, “Vectorizing cartoon animations,” *IEEE Transactions on Visualization and Computer Graphics (TVCG)*, vol. 15, no. 4, pp. 618–629, 2009.
- [4] J. Kopf and D. Lischinski, “Depixelizing pixel art,” in *ACM SIGGRAPH*, 2011, pp. 1–8.
- [5] M. Bessmeltsev and J. Solomon, “Vectorization of line drawings via polyvector fields,” *ACM Transactions on Graphics (TOG)*, vol. 38, no. 1, pp. 1–12, 2019.

- [6] G. Noris, A. Hornung, R. W. Sumner, M. Simmons, and M. Gross, “Topology-driven vectorization of clean line drawings,” *ACM Transactions on Graphics (TOG)*, vol. 32, no. 1, pp. 1–11, 2013.
- [7] G. Lecot and B. Levy, “Ardeco: Automatic region detection and conversion,” in *Eurographics Symposium on Rendering-EGSR*, 2006, pp. 349–360.
- [8] L. Donati, S. Cesano, and A. Prati, “An accurate system for fashion hand-drawn sketches vectorization,” in *Proceedings of the IEEE International Conference on Computer Vision (ICCV) Workshops*, Oct 2017.
- [9] E. A. Dominici, N. Schertler, J. Griffin, S. Hoshyari, L. Sigal, and A. Sheffer, “Polyfit: perception-aligned vectorization of raster clip-art via intermediate polygonal fitting,” *ACM Transactions on Graphics (TOG)*, vol. 39, no. 4, pp. 77–1, 2020.
- [10] Y. Ding, W. K. Wong, Z. Lai, and Z. Zhang, “Bilinear supervised hashing based on 2d image features,” *IEEE Transactions on Circuits and Systems for Video Technology (TCSVT)*, vol. 30, no. 2, pp. 590–602, 2019.
- [11] J. Yu, J. Li, Z. Yu, and Q. Huang, “Multimodal transformer with multi-view visual representation for image captioning,” *IEEE Transactions on Circuits and Systems for Video Technology (TCSVT)*, vol. 30, no. 12, pp. 4467–4480, 2019.
- [12] V. Egiastian, O. Voynov, A. Artemov, D. Volkhonskiy, A. Safin, M. Taktasheva, D. Zorin, and E. Burnaev, “Deep vectorization of technical drawings,” in *European Conference on Computer Vision (ECCV)*. Springer, 2020, pp. 582–598.
- [13] P. Reddy, M. Gharbi, M. Lukac, and N. J. Mitra, “Im2vec: Synthesizing vector graphics without vector supervision,” in *Proceedings of the IEEE/CVF International Conference on Computer Vision (CVPR)*, 2021, pp. 7342–7351.
- [14] J. Gao, C. Tang, V. Ganapathi-Subramanian, J. Huang, H. Su, and L. J. Guibas, “DeepSpline: Data-driven reconstruction of parametric curves and surfaces,” *arXiv:1901.03781*, 2019.
- [15] A. Sinha, A. Unmesh, Q. Huang, and K. Ramani, “Surfnet: Generating 3d shape surfaces using deep residual networks,” in *Proceedings of the IEEE/CVF International Conference on Computer Vision (CVPR)*, 2017, pp. 6040–6049.
- [16] C. Liu, J. Wu, P. Kohli, and Y. Furukawa, “Raster-to-vector: Revisiting floorplan transformation,” in *Proceedings of the IEEE International Conference on Computer Vision (ICCV)*, Oct 2017.
- [17] H. Su, J. Niu, X. Liu, Q. Li, J. Cui, and J. Wan, “Mangagan: Unpaired photo-to-manga translation based on the methodology of manga drawing,” in *Proceedings of the AAAI Conference on Artificial Intelligence (AAAI)*, vol. 35, no. 3, 2021, pp. 2611–2619.
- [18] H. Su, J. Niu, X. Liu, Q. Li, J. Wan, M. Xu, and T. Ren, “Artcoder: An end-to-end method for generating scanning-robust stylized qr codes,” in *Proceedings of the IEEE/CVF Conference on Computer Vision and Pattern Recognition (CVPR)*, 2021, pp. 2277–2286.
- [19] H. Su, J. Niu, X. Liu, Q. Li, J. Wan, and M. Xu, “Q-art code: Generating scanning-robust art-style qr codes by deformable convolution,” in *Proceedings of the 29th ACM International Conference on Multimedia (ACM MM)*, 2021, pp. 722–730.
- [20] X. Song, Y. Dai, and X. Qin, “Deeply supervised depth map super-resolution as novel view synthesis,” *IEEE Transactions on Circuits and Systems for Video Technology (TCSVT)*, vol. 29, no. 8, pp. 2323–2336, 2018.
- [21] J. Zhang, Y. Cao, Z.-J. Zha, Z. Zheng, C. W. Chen, and Z. Wang, “A unified scheme for super-resolution and depth estimation from asymmetric stereoscopic video,” *IEEE Transactions on Circuits and Systems for Video Technology (TCSVT)*, vol. 26, no. 3, pp. 479–493, 2014.
- [22] Q. Bo, W. Ma, Y.-K. Lai, and H. Zha, “All-higher-stages-in adaptive context aggregation for semantic edge detection,” *IEEE Transactions on Circuits and Systems for Video Technology (TCSVT)*, 2022.
- [23] Y. Liu, Q. Jia, X. Fan, S. Wang, S. Ma, and W. Gao, “Cross-srn: Structure-preserving super-resolution network with cross convolution,” *IEEE Transactions on Circuits and Systems for Video Technology (TCSVT)*, 2021.
- [24] Y. Guo, Z. Zhang, C. Han, W. Hu, C. Li, and T.-T. Wong, “Deep line drawing vectorization via line subdivision and topology reconstruction,” in *Computer Graphics Forum (CGF)*, vol. 38, no. 7. Wiley Online Library, 2019, pp. 81–90.
- [25] H. Mo, E. Simo-Serra, C. Gao, C. Zou, and R. Wang, “General virtual sketching framework for vector line art,” *ACM Transactions on Graphics (TOG)*, vol. 40, no. 4, pp. 1–14, 2021.
- [26] X. Ma, Y. Zhou, X. Xu, B. Sun, V. Filev, N. Orlov, Y. Fu, and H. Shi, “Towards layer-wise image vectorization,” in *Proceedings of the IEEE/CVF Conference on Computer Vision and Pattern Recognition (CVPR)*, 2022, pp. 16314–16323.

- [27] D. Ha and D. Eck, "A neural representation of sketch drawings," *arXiv:1704.03477*, 2017.
- [28] L. S. F. Ribeiro, T. Bui, J. Collomosse, and M. Ponti, "Sketchformer: Transformer-based representation for sketched structure," in *Proceedings of the IEEE/CVF Conference on Computer Vision and Pattern Recognition (CVPR)*, 2020, pp. 14 153–14 162.
- [29] R. G. Lopes, D. Ha, D. Eck, and J. Shlens, "A learned representation for scalable vector graphics," in *Proceedings of the IEEE/CVF International Conference on Computer Vision (CVPR)*, 2019, pp. 7930–7939.
- [30] A. Carlier, M. Danelljan, A. Alahi, and R. Timofte, "Deepsvg: A hierarchical generative network for vector graphics animation," *Advances in Neural Information Processing Systems*, vol. 33, pp. 16 351–16 361, 2020.
- [31] S. Azadi, M. Fisher, V. G. Kim, Z. Wang, E. Shechtman, and T. Darrell, "Multi-content gan for few-shot font style transfer," in *Proceedings of the IEEE conference on computer vision and pattern recognition (CVPR)*, 2018, pp. 7564–7573.
- [32] Y. Gao, Y. Guo, Z. Lian, Y. Tang, and J. Xiao, "Artistic glyph image synthesis via one-stage few-shot learning," *ACM Transactions on Graphics (TOG)*, vol. 38, no. 6, pp. 1–12, 2019.
- [33] T.-M. Li, M. Lukáč, M. Gharbi, and J. Ragan-Kelley, "Differentiable vector graphics rasterization for editing and learning," *ACM Transactions on Graphics (TOG)*, vol. 39, no. 6, pp. 1–15, 2020.
- [34] C. Li, X. Liu, and T.-T. Wong, "Deep extraction of manga structural lines," *ACM Transactions on Graphics (TOG)*, vol. 36, no. 4, pp. 1–12, 2017.
- [35] M. Xia, W. Hu, X. Liu, and T.-T. Wong, "Deep halftoning with reversible binary pattern," in *Proceedings of the IEEE/CVF International Conference on Computer Vision*, 2021, pp. 14 000–14 009.
- [36] M. Xie, M. Xia, X. Liu, C. Li, and T.-T. Wong, "Seamless manga inpainting with semantics awareness," *ACM Transactions on Graphics (TOG)*, vol. 40, no. 4, pp. 1–11, 2021.
- [37] M. Xie, M. Xia, and T.-T. Wong, "Exploiting aliasing for manga restoration," in *Proceedings of the IEEE/CVF Conference on Computer Vision and Pattern Recognition*, 2021, pp. 13 405–13 414.
- [38] M. Xie, C. Li, X. Liu, and T.-T. Wong, "Manga filling style conversion with screentone variational autoencoder," *ACM Transactions on Graphics (TOG)*, vol. 39, no. 6, pp. 1–15, 2020.
- [39] L. Zhang, C. Li, T.-T. Wong, Y. Ji, and C. Liu, "Two-stage sketch colorization," *ACM Transactions on Graphics (TOG)*, vol. 37, no. 6, pp. 1–14, 2018.
- [40] C. Han, Q. Wen, S. He, Q. Zhu, Y. Tan, G. Han, and T.-T. Wong, "Deep unsupervised pixelization," *ACM Transactions on Graphics (SIGGRAPH Asia 2018 issue)*, vol. 37, no. 6, pp. 243:1–243:11, November 2018.
- [41] X. Liu, T.-T. Wong, and P.-A. Heng, "Closure-aware sketch simplification," *ACM Transactions on Graphics (TOG)*, vol. 34, no. 6, pp. 1–10, 2015.
- [42] Y. Qu, W.-M. Pang, T.-T. Wong, and P.-A. Heng, "Richness-preserving manga screening," *ACM Transactions on Graphics (TOG)*, vol. 27, no. 5, pp. 1–8, 2008.
- [43] G. Wang, T.-T. Wong, and P.-A. Heng, "Deringing cartoons by image analogies," *ACM Transactions on Graphics (TOG)*, vol. 25, no. 4, pp. 1360–1379, 2006.
- [44] A. Shesh and B. Chen, "Efficient and dynamic simplification of line drawings," in *Computer Graphics Forum*, vol. 27, no. 2. Wiley Online Library, 2008, pp. 537–545.
- [45] G. Noris, D. Šykora, A. Shamir, S. Coros, B. Whited, M. Simmons, A. Hornung, M. Gross, and R. Sumner, "Smart scribbles for sketch segmentation," in *Computer Graphics Forum*, vol. 31, no. 8. Wiley Online Library, 2012, pp. 2516–2527.
- [46] A. Plaata, W. Kosters, and M. Preuss, "Model-based deep reinforcement learning for high-dimensional problems, a survey," *arXiv preprint arXiv:2008.05598*, 2020.
- [47] T. P. Lillicrap, J. J. Hunt, A. Pritzel, N. Heess, T. Erez, Y. Tassa, D. Silver, and D. Wierstra, "Continuous control with deep reinforcement learning," *arXiv:1509.02971*, 2015.
- [48] V. Konda and J. Tsitsiklis, "Actor-critic algorithms," *Advances in neural information processing systems*, 2000.
- [49] Z. Huang, W. Heng, and S. Zhou, "Learning to paint with model-based deep reinforcement learning," in *Proceedings of the IEEE/CVF International Conference on Computer Vision (CVPR)*, 2019, pp. 8709–8718.
- [50] K. He, X. Zhang, S. Ren, and J. Sun, "Deep residual learning for image recognition," in *Proceedings of the IEEE conference on computer vision and pattern recognition (CVPR)*, 2016, pp. 770–778.
- [51] S. Ioffe and C. Szegedy, "Batch normalization: Accelerating deep network training by reducing internal covariate shift," in *International conference on machine learning (ICML)*. PMLR, 2015, pp. 448–456.
- [52] T. Salimans and D. P. Kingma, "Weight normalization: A simple reparameterization to accelerate training of deep neural networks," *Advances in neural information processing systems (NIPS)*, vol. 29, pp. 901–909, 2016.
- [53] Adobe, "Adobe illustrator," *Image Trace*, <http://www.adobe.com/>, 2021.
- [54] P. Selinger, "Potrace: a polygon-based tracing algorithm," *Potrace (online)*, <http://potrace.sourceforge.net/potrace.pdf> (2009-07-01), vol. 2, 2003.
- [55] C.-Y. Yao, S.-H. Hung, G.-W. Li, I.-Y. Chen, R. Adhitya, and Y.-C. Lai, "Manga vectorization and manipulation with procedural simple screentone," *IEEE transactions on visualization and computer graphics*, vol. 23, no. 2, pp. 1070–1084, 2016.
- [56] Kozea, "Cairosvg," <https://cairosvg.org/>.
- [57] Z. Wang, A. C. Bovik, H. R. Sheikh, and E. P. Simoncelli, "Image quality assessment: from error visibility to structural similarity," *IEEE Transactions on Image Processing (TIP)*, vol. 13, no. 4, pp. 600–612, 2004.
- [58] J.-D. Favreau, F. Lafarge, and A. Bousseau, "Fidelity vs. simplicity: a global approach to line drawing vectorization," *ACM Transactions on Graphics (TOG)*, vol. 35, no. 4, pp. 1–10, 2016.
- [59] S. McKinley and M. Levine, "Cubic spline interpolation," *College of the Redwoods*, vol. 45, no. 1, pp. 1049–1060, 1998.
- [60] Z. Liu, H. Li, W. Zhou, T. Rui, and Q. Tian, "Making residual vector distribution uniform for distinctive image representation," *IEEE Transactions on Circuits and Systems for Video Technology (TCSVT)*, vol. 26, no. 2, pp. 375–384, 2015.
- [61] C.-Y. Yao, K.-Y. Chen, H.-N. Guo, C.-C. Li, and Y.-C. Lai, "Resolution independent real-time vector-embedded mesh for animation," *IEEE Transactions on Circuits and Systems for Video Technology (TCSVT)*, vol. 27, no. 9, pp. 1974–1986, 2016.



Hao Su is a Ph.D. student in State Key Laboratory of Virtual Reality Technology and Systems, Beihang University, China. He received the B.E. degree in Computer Science and Technology from Zhengzhou University, in 2016. His research interests are in deep learning, computer graphics, and image processing.



Xuefeng Liu received the M.S. and Ph.D. degrees from the Beijing Institute of Technology, China, and the University of Bristol, United Kingdom, in 2003 and 2008, respectively. He was an associate professor at the School of Electronics and Information Engineering in the HuaZhong University of Science and Technology, China from 2008 to 2018. He is currently an associate professor at the School of Computer Science and Engineering, Beihang University, China. His research interests include wireless sensor networks, distributed computing and network processing. He has served as a reviewer for several international journals/conference proceedings.



Jianwei Niu received the M.S. and Ph.D. degrees in computer science from Beihang University, Beijing, China, in 1998 and 2002, respectively. He was a visiting scholar at School of Computer Science, Carnegie Mellon University, USA from Jan. 2010 to Feb. 2011. He is a professor in the School of Computer Science and Engineering, BUAA, and an IEEE senior member. His current research interests include mobile and pervasive computing, mobile video analysis.



Jiahe Cui is currently working toward the PhD degree in college of computer and science at Beihang University, Beijing, China. His research interests are multi-sensor SLAM and perceptual algorithms in autonomous driving.



Ji Wan is currently working toward the PhD degree at the State Key Laboratory of Software Development Environment, Beihang University. His research interests include distributed systems and blockchain.



Xinghao Wu is currently working toward the PhD degree in the school of computer science and engineering, Beihang University. His research interests are federated learning and distributed machine learning.